On electrostatic and Casimir force measurements between conducting surfaces in a sphere-plane configuration

W.J. Kim*,[1] M. Brown-Hayes,[1] D.A.R. Dalvit,[2] J.H. Brownell,[1] and R. Onofrio[3,1]

[1] *Department of Physics and Astronomy, Dartmouth College, 6127 Wilder Laboratory, Hanover, NH 03755, USA*

[2] *Theoretical Division, MS B213, Los Alamos National Laboratory, Los Alamos, NM 87545, USA*

[3] *Dipartimento di Fisica "Galileo Galilei", Università di Padova, Via Marzolo 8, Padova 35131, Italy*

(Dated: December 1, 2008)

We report on measurements of forces acting between two conducting surfaces in a spherical-plane configuration in the 35 nm-1 μm separation range. The measurements are obtained by performing electrostatic calibrations followed by a residuals analysis after subtracting the electrostatic-dependent component. We find in all runs optimal fitting of the calibrations for exponents smaller than the one predicted by electrostatics for an ideal sphere-plane geometry. We also find that the external bias potential necessary to minimize the electrostatic contribution depends on the sphere-plane distance. In spite of these anomalies, with a proper but model-dependent subtraction of the electrostatic contribution we have found evidence for short-distance attractive forces of magnitude comparable to the expected Casimir-Lifshitz force. We finally discuss the relevance of our findings in the more general context of Casimir-Lifshitz force measurements, with particular regard to the critical issues of the electrical and geometrical characterization of the involved surfaces.

PACS numbers: 12.20.Fv, 03.70.+k, 04.80.Cc, 11.10.Wx

I. INTRODUCTION

Casimir-Lifshitz forces [1, 2] provide an experimental window on the nature of quantum vacuum at the macroscopic level [3, 4, 5, 6, 7, 8, 9, 10, 11]. After pioneering attempts in the original parallel plate configuration [12], and in a variant of this configuration based upon a sphere and a plane [13], the claimed accuracy of recent experiments ranges from 15% in the parallel plane case [14] to 0.2-5% in the sphere-plane case [15, 16, 17, 18, 19]. In the case of the sphere-plane configuration, the Casimir force is typically evaluated by using the so-called proximity force approximation (PFA) [20, 21], introducing a theoretical uncertainty estimated to be in the 0.1 % range, and recently investigated experimentally [22].

A sphere-plane experiment has been performed, with a radius of curvature for the sphere of order of cm, at relatively large distances above 1μm [15]. In this case the largest deviation from the bare Casimir formula for an idealized configuration (perfect conductors, zero temperature) is expected to be the thermal contribution to the radiation pressure on the surfaces, still below the sensitivity of the apparatus at the largest explored distances. Three sphere-plane experiments have also been performed in a quite distinct regime, with smaller radius of curvature, of order 100 μm, and in the range below one micrometer [16, 17, 18, 23]. At distances less than 1 μm the correction to the Casimir force due to finite conductivity and surface roughness of the substrates cannot be neglected at the level of accuracy claimed in these three experiments. At least other five groups have recently performed Casimir force experiments in the sphere-plane configuration [24, 25, 26, 27, 28].

Mastering the Casimir force at the highest level of accuracy is essential to provide reliable limits to other macroscopic forces acting in the micrometer range, such as corrections to the Newtonian gravitational force independently predicted in many attempts to unify gravitation with the remaining fundamental interactions [29, 30, 31]. Although in the nanometer range the Casimir force loses its universal nature morphing into more specific, structure-dependent, molecular van der Waals forces, its study is sometimes considered of some relevance for designing nanomechanical structures and to investigate nonlinear effects, as first discussed in [32] and then experimentally demonstrated in [33, 34].

In this paper we report more extensively on measurements performed in a sphere-plane geometry exploring a novel range of parameters that interpolates between the two previous sets of sphere-plane measurements [35]. We use a gold-coated spherical lens with large radius of curvature, similar to the experiment performed by Steve Lamoreaux in Seattle, while at the same time exploring distances down to few tens of nanometers from the point of contact between the sphere and the plane, similar to more microscopic setups using microresonators. While we do achieve some evidence for the expected Casimir-Lifshitz force, our measurements suggest that a reanalysis of systematic effects in previous experiments will be beneficial to assess the accuracy with which this force has been measured so far, with particular regard to the role of the residual electrostatic forces [36, 37].

The paper is organized as follows: in Section II we describe the experimental apparatus and the basics of our

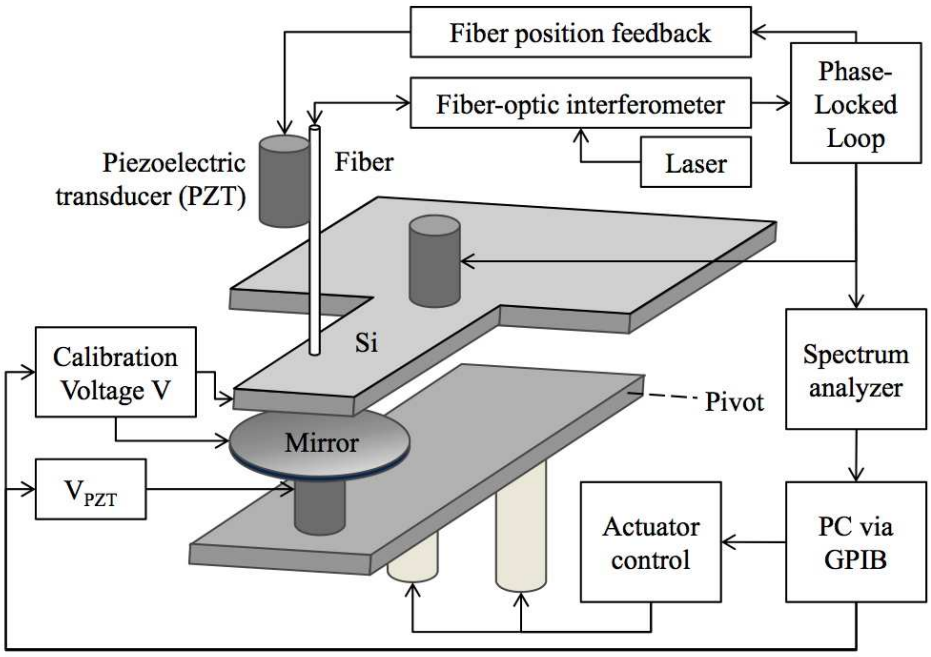

FIG. 1: Schematic of the experimental setup and the data acquisition scheme. The silicon resonator is opposed by a spherical mirror, both Au coated. The latter can be moved along the vertical direction by driving two mechanical actuators for coarse approach, and with a piezoelectric actuator for fine control of the separation. The outside face of the resonator reflects light coming from a fiber optic interferometer, located 20-100 μm above it. The resonator is driven weakly at its resonant frequency with a piezoelectric actuator connected in a phase-locked loop (PLL) to the optical fiber.

measurement technique. In Section III we describe a procedure for electrostatic calibrations to determine various critical parameters such as the calibration factor, the absolute separation, and the minimizing potential related to the contact potential. Careful control over the system parameters allows us to search for a non-Coulombian contribution to the observed force signal and therefore to test this residual against various hypothesis such as a possible uncompensated electrical voltage, and the presence of the Casimir-Lifsthiz force, as described in Section IV. In Section V we critically assess systematic effects in our measurements and compare our findings to both previous short-range Casimir force measurements and long-range atomic force microscopy measurements.

II. EXPERIMENTAL SET-UP

The experimental setup is an upgrade of the one already described in a previous paper [38] for measuring the Casimir force in the cylinder-plane configuration as first theoretically discussed in [39]. Forces acting between a flat surface and a spherical surface are detected by measuring the shift in the mechanical oscillation frequency of a silicon cantilever that acts as the plane surface. The main components in this setup are the use of a phase-locked loop scheme [40] to drive the cantilever at its resonant frequency, the use of optical quality surfaces for both the resonator and the sphere, and a faster and more flexible data acquisition scheme.

A schematic of the apparatus is shown in Fig. 1. The rectangular cantilever, of length $L = (22.56 \pm 0.01)$ mm, width $w = (9.93 \pm 0.01)$ mm and thickness $t = (330 \pm 10)$ μm was laser-cut from a silicon wafer. Given the density of silicon, $\rho = 2.3 \times 10^3$ kg/m^3, the physical mass of the cantilever is $m_p = (1.72 \pm 0.05) \times 10^{-4}$ kg. The cantilever is sandwiched between two aluminum clamping structures, electrically isolated and thermally stabilized by a Peltier cooler. This last feature is required since we have observed that the resonant frequency of the cantilever drifts as much as 2 Hz as the ambient temperature fluctuates about 1 K over the duration of a typical run of a few hours. The effect of the thermal drifts has also been mitigated off-line by a proper implementation of the data acquisition

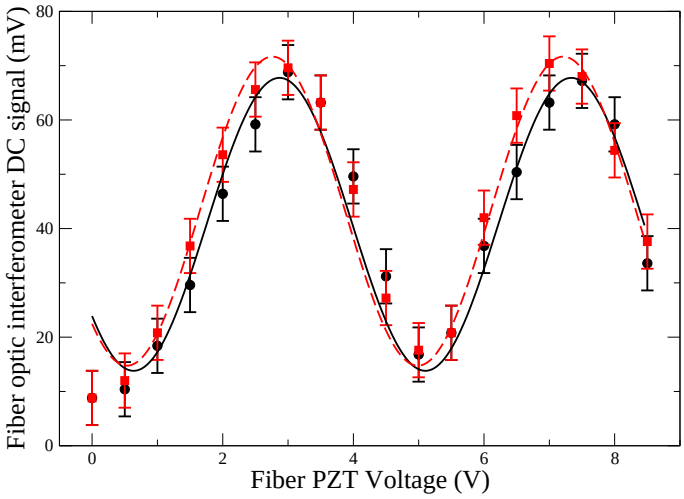

FIG. 2: Calibration of the PZT actuator governing the sphere-plane separation. Four calibrations of the PZT actuator have been performed during the overall data taking, of which only two are reported here for simplicity, indicated with red-square and black-dot points, and their best fit with a sinusoidal function (red, dotted line, and black, continuous line, respectively). The average value of the actuation coefficient from the four data sets is $\beta = (87 \pm 2)$ nm/V.

sequence, as described in Section III.

Below the cantilever a spherical mirror with radius of curvature $R = (30.9 \pm 0.15)$ mm and diameter $a = (8.00 \pm 0.25)$ mm is mounted on an aluminum frame connected to two motorized actuators allowing for coarse translational motion, plus an additional piezoelectric transducer for fine translational motion driven with a bias $V_{\rm PZT}$. The spherical lens is gold-coated by the manifacturing company with a thickness of 250 nm ($\pm$ 10 %) The surface of the cantilever facing the spherical lens is coated with a 200 nm layer of gold ($\pm$ 10 %) by thermal evaporation, with the rate of evaporation kept below 50 $\mathring{A}$/sec at a pressure of 3×10^{-6} mbar to ensure better conditions for homogeneous coating.

The predicted frequency of the fundamental flexural mode of the cantilever is $\nu_p = (0.162t/L^2)\sqrt{E/\rho}$ with E the Young's modulus of the material [41]. In our case this yields a resonant frequency around 894 Hz, within few percent from the measured frequency at the typical vacuum pressure of 1.6×10^{-4} Torr in the vacuum chamber. The stiffness k of the resonator can be estimated by assuming an effective mass for the resonator mode roughly equal to the physical mass, which yields $k = 1.036Ewt^3/L^3 \simeq 5.4 \times 10^3$ N/m. The stiffness is three or four orders of magnitude higher than the typical cantilevers used in atomic force microscopy, implying both advantages and drawbacks. A large stiffness allows us to reliably achieve small gaps with little static deflection of the cantilever in the presence of strong electric fields for calibration purposes, at the expense of a lower force sensitivity. By decreasing the stiffness of the cantilever both the reachable minimum gap before snapping between the two surfaces occurs and the largest explorable gap for a given signal to noise ratio are increased.

The motion of the cantilever is detected by using a fiber optic interferometer [42] positioned a few microns above the upper cantilever face and fed by temperature-stabilized diode laser with an adjustable power in the 5-10 mW range at the wavelength of 781 nm. The output signal from the interferometer is filtered and amplified through a single reference mode lock-in amplifier and is fed back into the piezoelectric actuator driving the cantilever motion. The phase between the input and the output signals is properly chosen to maximize the vibration amplitude, typically around 30-40 degrees. This scheme is much faster and more efficient than the previous open-loop scheme as described in [38] in which white noise was used as the driving source without a feedback, and the complete FFT spectrum was acquired. The vibration frequency was measured by a counter with 10 mHz resolution, 100 times faster than in the open-loop scheme. The front side of the chamber has a large viewport allowing for visual inspection of the relevant components through an optical microscope, as shown in Fig. 10 of [38]. This also provides for a quick assessment of the optical fiber location, which can be manually adjusted within few hundred micrometers from the underlying resonator using a feedthrough micrometer.

The PZT was calibrated by using the same fiber optic interferometer with the cantilever removed and the spherical mirror replaced by a flat mirror. Assuming a linear relationship $\Delta x = \beta \Delta V_{\rm PZT}$, the DC interference amplitude versus the voltage applied to the PZT, as shown in Fig. 2, was fit with a sinusoidal function and the distance inferred from

its period to be half of the 781 nm laser wavelength. The average of four separate calibration runs yields $\beta = (87 \pm 2)$ nm/V, and it was found to be independent of the voltage applied to the PZT, within the error, in the 0-100 V range. The sensitivity of the fiber optic interferometer is evaluated in the same configuration by driving the PZT with a monoschomatic signal at various amplitudes, and looking the corresponding signal at the FFT spectrum analyzer. When the driving amplitude at a frequency of 1 KHz (still well below the maximum response frequency of the PZT of 69 KHz) is reduced at the level of a peak-to-peak signal of 0.25 mV, the measured amplitude at the FFT spectral analyzer becomes equal to the FFT broadband noise level of 10 $\mu V_{\rm rms}$ with an integration time of 10 s. Using the determined value of the actuation coefficient of the PZT, we estimate the minimum detectable signal with SNR $\simeq 1$ to be $\simeq 0.80 \mathring{A}/\sqrt{\rm Hz}$, similar to the one reported in [42].

For a generic distance-dependent force and for a small amplitude of the cantilever oscillation (2-3 nm as inferred from the interferometer signal) with respect to the average separation between the two surfaces x, the measured frequency of the resonator ν_m is shifted with respect to the proper frequency of the resonator ν_p in such a way that

$$\Delta\nu^2 = \nu_m^2 - \nu_p^2 = -\frac{1}{4\pi^2 m_{\rm eff}} \frac{\partial F(x)}{\partial x}, \tag{1}$$

where $m_{\rm eff}$ is the effective mass of the mode of oscillation of the resonator. In general, the total force acting on the resonator is the aggregate from independent sources and the square of the measured frequency ν_m of a cantilever can be identified as the sum of contributions from those sources,

$$\nu_m^2(x,V) = \nu_p^2 + \Delta\nu_e^2(x,V) + \Delta\nu_r^2(x), \tag{2}$$

where $\Delta\nu_e^2$ is the frequency shift due to electrical force gradients for instance due to an external bias voltage V, and $\Delta\nu_r^2$ is the frequency shift subject to force gradients of non-electrostatic nature, for instance the Casimir force, or random drifts of instrumental and environmental origin. In the next section we will discuss the response of the resonator in the case of electrostatic forces.

III. ELECTROSTATIC CALIBRATIONS

We start with the electrostatic energy stored in a generic capacitance $C(x)$ biased by an external potential V, and under the presence of a contact potential $V_c(x)$ which in general may depend on the distance:

$$E_{el} = \frac{C(x)}{2}[V - V_c(x)]^2. \tag{3}$$

As recently pointed out by Lamoreaux [43], if the contact potential depends on distance the electrostatic force will include an additional term independent upon the external bias voltage. Since in our configuration the observable is the frequency shift, proportional to the second derivative of the electrostatic energy with respect to x, we have, after regrouping the various terms in powers of $V - V_c$:

$$E''_{el} = \frac{C''}{2}(V - V_c)^2 - [2C'V'_c + CV''_c](V - V_c) + CV_c'^2. \tag{4}$$

This can be regrouped again as $E''_{el} = A(V - V_c + B)^2 + D$ and, identifying the coefficients A, B, D to match the terms in Eq. 4, we obtain

$$A = \frac{C''}{2} \quad , \quad B = -\frac{2C'V'_c + CV''_c}{C''} \quad , \quad D = CV_c'^2 - \frac{(2C'V'_c + CV''_c)^2}{2C''}. \tag{5}$$

This allows to write:

$$E''_{el} = \frac{C''}{2}(V - V_0)^2 + CV_c'^2 - \frac{(2C'V'_c + CV''_c)^2}{2C''}, \tag{6}$$

where

$$V_0(x) = V_c(x) + \frac{2C'V'_c + CV''_c}{C''} \tag{7}$$

is the *minimizing* external potential, *i.e.* the external bias minimizing the electrostatic contribution to the frequency shift. It is clear that, even if the external bias voltage is chosen to minimize the electrostatic contribution, an

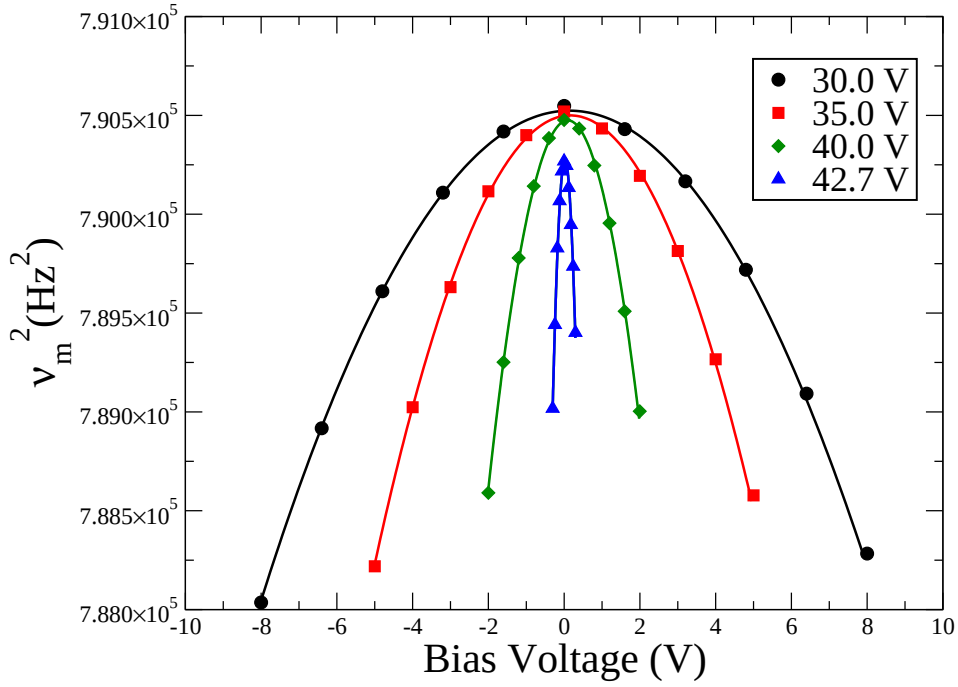

FIG. 3: Parabolic dependence of the squared frequency ν_m^2 upon the external bias voltage V for a typical experimental run. The different curves correspond to different values of the sphere-plane separation (defined in the legend in terms of the voltage applied to the PZT used for approaching the sphere). The range of external bias voltages is adapted for each sphere-plane separation to maintain comparable values of the maximum detected frequency shift, of about 1 Hz. This corresponds to keep a constant value for the electric field in the gap. The best fit with a parabolic function is also shown, with the parabolic curves relative to the largest PZT voltages (corresponding to smaller gap separations) displaying largest curvatures. No significant dependence of the fitting parameters has been observed by changing the external bias voltage span.

irreducible term containing the first and second spatial derivatives of V_c in Eq. 7 still causes a frequency shift. The expected frequency shift due to Coulombian interactions is therefore:

$$\nu^2 = {\nu_0}^2 - \frac{C''}{8\pi^2 m_{\rm eff}}(V - V_0)^2 + \frac{1}{4\pi^2 m_{\rm eff}}\left[-C{V_c'}^2 + \frac{(2C'V_c' + CV_c'')^2}{2C''}\right]. \tag{8}$$

We identify three contributions on the RHS of Eq. 8: the first term is unrelated to external or internal voltages, the second term depends on the external voltage, and the last term is a Coulombian contribution only related to the spatial dependence of the contact potential. The electrostatic calibrations consist in the study of the response of the cantilever frequency to an external potential, therefore selecting the second contribution alone which allows to infer both the effective mass of the resonator and the minimizing potential V_0. This knowledge is then used to infer the contact potential assuming a specific form of the functional dependence on distance of V_0, which is in turn used to identify the third contribution in Eq. 8. The subtraction of the total Coulombian contribution allows then to evaluate the square frequency related to non-Coulombian forces and to random drifts due to background noise in the apparatus (see section IV) as first discussed in AFM measurements by [44] and in the specific context of Casimir measurements in [45].

Regarding the capacitance, for the sphere-plane configuration and for our choice of parameters, the proximity force approximation (PFA) holds and the capacitance is $C(x) = 2\pi\epsilon_0 R \ln(R/x)$. This formula in principle must be corrected for the finite spherical mirror diameter used in alternative to a full sphere, but this is a sub-leading PFA correction approximately equal to 0.1% for a typical separation of $d = 1\mu$m. Therefore, the measured frequency ν_m of the cantilever can be parameterized as

$$\nu_m^2(x) = \nu_0^2(x) - K_{\rm el}(x)(V - V_0)^2, \tag{9}$$

where $\nu_0^2(x) = \nu_p^2 + \Delta\nu_e^2(x, V_0) + \Delta\nu_r^2(x)$, a parabola whose maximum is reached when the applied voltage at a given

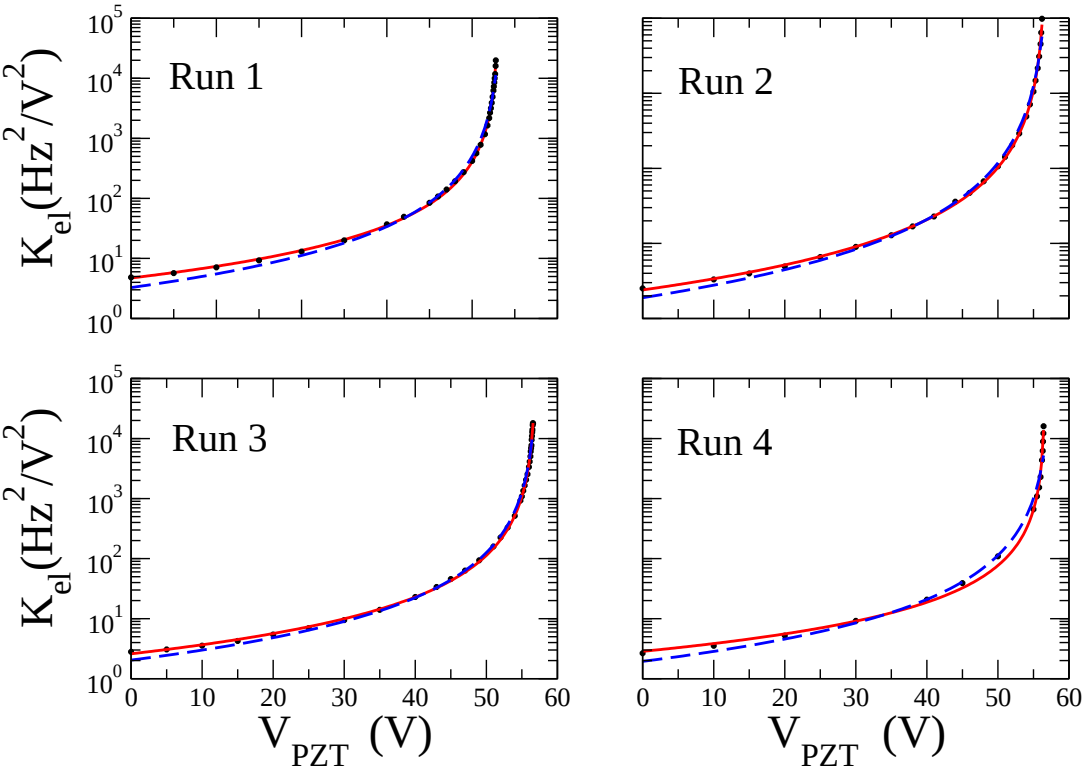

FIG. 4: Electrostatic curvature coefficient versus the voltage applied to the PZT actuator for four different runs, and related fits with the expected fixed exponent $e = -2$ (blue dashed line) as in Eq. 10 and by allowing the exponent to be a free parameter (red continuous line). In run 1 the location of the surface of the sphere in proximity of the cantilever is different from the other runs, as the latter were taken after tilting the sphere by an angle equal to 5×10^{-2} radians.

distance equals to the minimizing potential V_0. The parabola curvature $K_{\rm el}(x) = \epsilon_0 R/4\pi m_{\rm eff} x^2$ reflects the cantilever response to externally applied electric forces at a given distance x and allows to extract the effective mass of the resonator mode, and it can be measured by sweeping the applied bias over a bipolar range to discern the parabolic dependence of the frequency shift. The minimizing potential V_0 is found by looking at the horizontal displacement of the parabola. In Fig. 3 we show examples of electrostatic calibrations in which the square resonator frequency is plotted versus the bias voltage for different values of the gap separation between the sphere and the plane. In order to minimize the resonator frequency drifts due to fluctuations of ambient temperature, we measure the unbiased frequency before and after each measurement taken at a given bias voltage V. The average of the two unbiased frequencies is then used as the reference to evaluate the shift. We notice two remarkable features in Fig. 3. First, the peak value of the frequency is different in the four cases, reflecting the possible presence of a distance-dependent force combined with possible drifts in the value of the intrinsic frequency. Second, the location of the peak value of the resonator frequency in the parabolic fit does not occur at the same value of external voltage, indicating a distance-dependent minimizing potential.

The absolute distance between the sphere and the plane is not known with sufficient accuracy prior to the force measurement. In the experiment, the gap is varied by the voltage applied to the PZT ($V_{\rm PZT}$) and consequently $K_{\rm el}$ is a function of the relative distance (*i.e.*, of the applied $V_{\rm PZT}$). This requires an additional fitting parameter $V^0_{\rm PZT}$, which would cause contact and must be inferred from fitting the function

$$K_{\rm el}(V_{\rm PZT}) = \alpha(V^0_{\rm PZT} - V_{\rm PZT})^{-2}, \tag{10}$$

where α is a calibration factor containing the effective mass of the cantilever through $\alpha \equiv \epsilon_0 R/4\pi m_{\rm eff}\beta^2$. In Fig. 4 the curvature parameter $K_{\rm el}$ is plotted versus the piezoelectric actuator voltage $V_{\rm PZT}$ for four different experimental runs. Assuming the PZT actuation is linear, the absolute separation for a given $V_{\rm PZT}$ can be inferred in two ways: $x(V_{\rm PZT}) = \beta(V^0_{\rm PZT} - V_{\rm PZT})$ or $x(V_{\rm PZT}) = \beta[\alpha/K_{\rm el}(V_{\rm PZT})]^{1/2}$. Therefore, the absolute distance can be inferred either

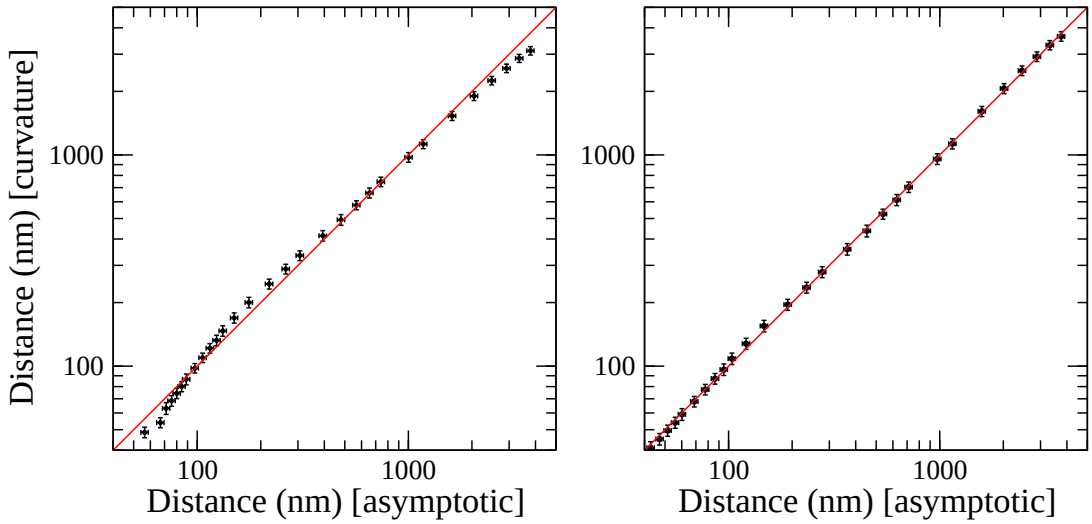

FIG. 5: Plot of $x(V_{\rm PZT})$ converted into distance, as evaluated from the calibration factor α for the inverse square law, versus the same function evaluated from the asymptotic limit of the fit function. The left plot uses the expected electrostatic law with an exponent $e = -2$, while the right plot is obtained by optimizing the exponent in the curvature scaling with distance. Red lines are added to provide an eyeguide for the deviations from the expected consistency between the two determinations of the same quantity.

from the asymptotic limit $V^0_{\rm PZT}$ of the fit function or from the calibration factor α of the same function, indicating an interdependency of the two physical parameters appearing in Eq. (10). Note that quite large values of $K_{\rm el}$, of order $-2 \times 10^4 {\rm Hz}^2/{\rm V}^2$ in runs 1, 3, and 4, have been achieved. These large signals serve to accurately constrain the fit parameters owing to the high stiffness of the cantilever, which allows us to explore very small distances between the sphere and the cantilever without stiction.

Comparison of the two methods for determining $x(V_{\rm PZT})$ in Fig. 5 (left plot) reveals disagreement when applying the inverse square law in Eq. 10. Direct measurement of the sphere-plane capacitance versus gap provides a third assessment of $V^0_{\rm PZT}$. In Fig. 6 the capacitance versus PZT voltage is shown with the fitting curve corresponding to the capacitance between a sphere and a plane in the PFA approximation.

Another issue complicating the electrostatic calibrations is evident in Fig. 7 displaying V_0 inferred from Fig. 3 versus $V_{\rm PZT}$. While the error bars are relatively large at large gap separations, they become smaller at smaller gaps, and two distinct dependencies are observed. In runs 1 and 2 the minimizing potential seems to depend linearly on the gap separation at small separations, while in the remaining runs it appears to tend towards a constant value. The significance of this dependence in the context of high-precision measurements of the Casimir force is discussed in section V.

The error in the curvature parameter $K_{\rm el}$ has been determined with dedicated runs in which conditions nominally leading to the same gap size are maintained, and the result is shown in Fig. 8. The overall time drift in $K_{\rm el}$, if converted into a thermally induced change in gap size, corresponds to ± 200 nm. The average random uncertainty in $K_{\rm el}$ has been evaluated by taking the data of Fig. 8 and subtracting for each point the long term drift by means of a moving average with a defined time window. By choosing the average time window equal to 4 curvature measurements (each measurement taking 8-10 minutes depending on the number of points obtained in the frequency versus bias voltage measurement) we obtain a relative error in $K_{\rm el}$ equal to about 4% error on top of the fitting uncertainty associated with the parabolic fit. This allows us to quantitatively compare fitting functions for the distance dependence of $K_{\rm el}$, and has resulted in another anomalous behavior. Indeed, the reduced χ^2 is near one when the exponent is fit in the -1.7 to -1.8 range, while it is at least one order of magnitude higher for fixed -2.0 exponent, as shown in Table 1.

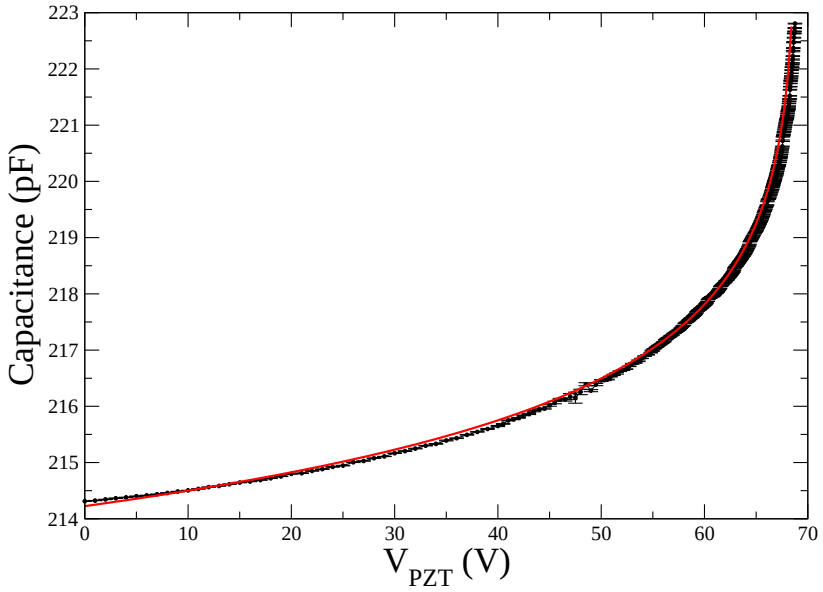

FIG. 6: Capacitance versus PZT voltage data (black circles) and its best fit (red line). The fit is based on the PFA formula $C(d) = C_0 + A\ln[\beta(V^0_{\rm PZT} - V_{\rm PZT})]$, where the actuation coefficient $\beta = (87 \pm 2)$ nm/V. The best fit yields, for the coefficients C_0 and A, the values $C_0 = (193.9 \pm 0.2)$ pF and $A = -(1.757 \pm 0.002)$ pF, this last in agreement within two standard deviations with the less accurate theoretical expectation $A = -2\pi\epsilon_0 R = -(1.72 \pm 0.02)$ pF. The same fit provides a value for the asymptotic value of the PZT voltage corresponding to zero gap distance the value $V^0_{\rm PZT} = (69.31 \pm 0.01)$ Vm, equivalent to a distance of 47 ± 2 nm. The best fit corresponds to a reduced $\chi^2 = 2.9$.

Adherence of our data to a strict power law from the farthest to the closest approach in all four cases implies the drift played little role during our data runs, except possibly in the case of Run 4. However, we find that the data clearly *fail* to follow the inverse square law dependence of the electrostatic coefficient upon the sphere-plane separation. More quantitatively, if the fitting exponent is left as a free parameter, our experimental data from four separate sequences follow a power law with exponents $-1.70 \pm 0.01, -1.77 \pm 0.02, -1.80 \pm 0.01, -1.54 \pm 0.02$, far from the expected value of -2. When substituted into Eq. 10, these exponent values produce better agreement between the two methods for determining $x(V_{\rm PZT})$, as shown in the right plot in Fig. 5.

The stability of the electrostatic result has been checked through repeating the data fit of $K_{\rm el}$ versus $V_{\rm PZT}$, starting with few points at the largest distances and by progressively including the data point corresponding to the closer

	Run 1	Run 2	Run 3	Run 4
fixed exponent	-2	-2	-2	-2
α (Hz^{2}V^{-2}m^2)	6200 ± 98	6197 ± 97	6701 ± 101	6438 ± 156
x_0 (nm)	64.4 ± 1.7	90.5 ± 2.6	62.6 ± 1.7	93.1 ± 2.6
χ^2/DOF	15.9	7.7	6.9	36.5
free exponent	-1.70 ± 0.01	-1.77 ± 0.02	-1.80 ± 0.01	-1.54 ± 0.02
α (Hz^{2}V^{-2}m^e)	2805 ± 92	3021 ± 153	3732 ± 144	1415 ± 69
x_0 (nm)	29.6 ± 0.9	49.6 ± 1.7	35.7 ± 1.7	20.0 ± 1.7
χ^2/DOF	1.0	0.8	1.2	7.0

TABLE I: Fitting parameters of the electrostatic calibrations, and values of the reduced χ^2, as the absolute χ^2 normalized by the number of degrees of freedom (DOF) in the fitting for a fixed exponent equal to 2 as expected from electrostatic considerations, and for a free exponent e. Note that the calibration factor α characterizes the sensitivity of our apparatus, yielding the effective mass in the case of fitting with the expected Coulomb exponent equal to 2. Variations of α from run to run are attributable to the rearrangement of the resonator clamping system, which strongly affects its effective mass. If the exponent is different from the expected value of 2, then the dimension of α changes and the effective mass cannot be properly evaluated.

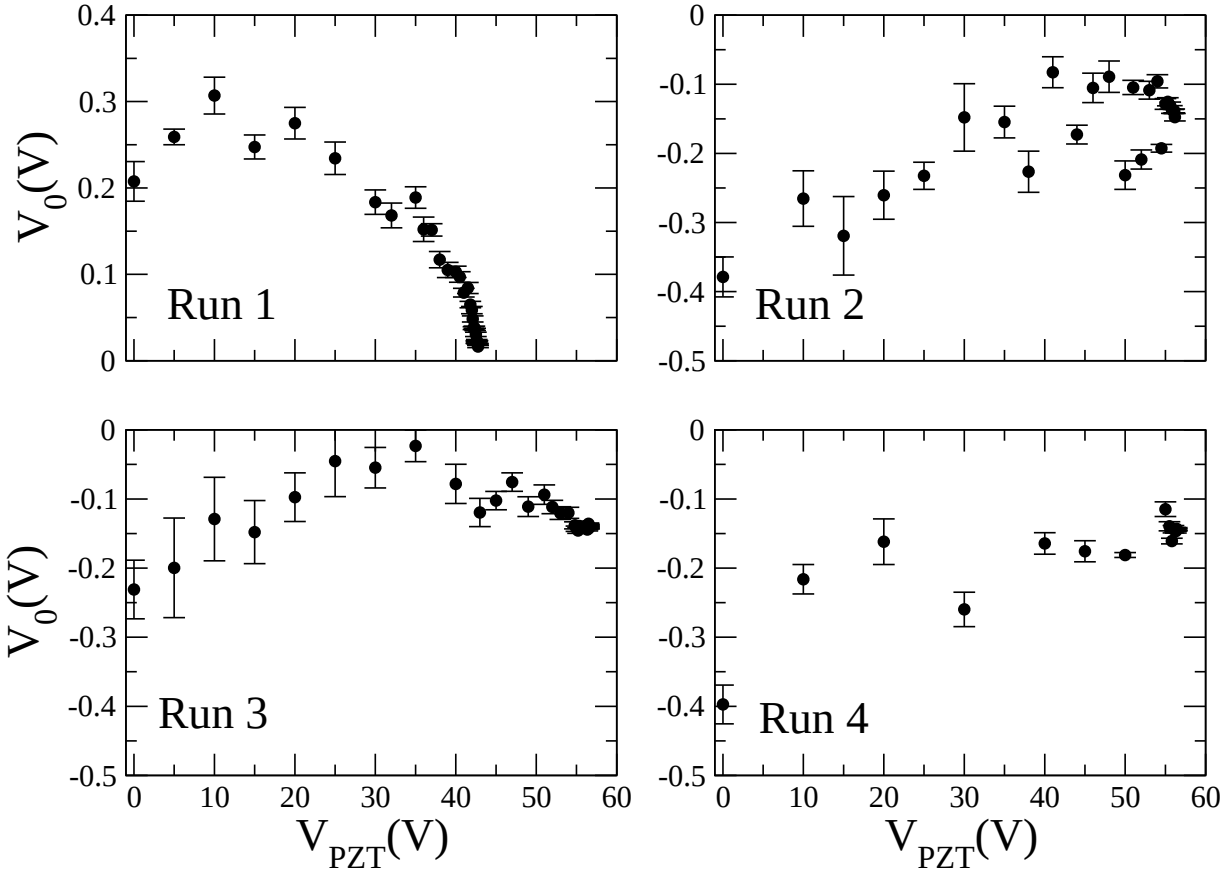

FIG. 7: Plot of the minimizing potential versus $V_{\rm PZT}$ for the same four runs shown in Fig. 4. Two behaviors are evident at small separation (large $V_{\rm PZT}$): either an approximately constant potential (Run 3 and Run 4) or a potential linearly dependent upon the separation (Run 1 and, to a less extent, Run 2). Note that in run 1 V_0 is positive while for Runs 2-4 it is negative and converges to $V_0 \simeq$ -150 mV at the smallest separations.

distances. In this way the intrinsic instability of the fit will manifest itself through a systematic variation in the fit parameters subject to a choice of data points included. Figures 9 and 10 show the result of the stability test for Run 1-4, revealing dependence of the fits on the number of points considered. As we will discuss later in Section IV, this is limiting the accuracy of the determination of the Casimir force. In Table 1 we report the values of the parameters of the best fit of the electrostatic calibration for the four runs, leaving the exponent free, and with the exponent frozen at the expected value of -2. In the latter case one can infer the effective mass of the cantilever and this turns out to be larger by an order of magnitude than the physical mass, against the expectation to be a fraction of the physical mass [46, 47, 48]. Apart from the uncertainties related to the clamping of the resonator, this is another signal that the calibration fitting with a pure electrostatic contribution neglects some systematic effect.

The unexpected power law poses a significant limit on the validity of our electrostatic calibration. Among the possible systematic effects causing this deviation from the expected Coulombian behaviour, we have considered the following.

A. Static deflection of cantilever

The spring constant of our cantilever is extremely stiff (about 5400 N/m). Using Hooke's law, a deflection experienced by the cantilever due to an electrostatic force at 100 nm with an applied voltage of 100 mV is less than 0.2 $\mathring{A}$.

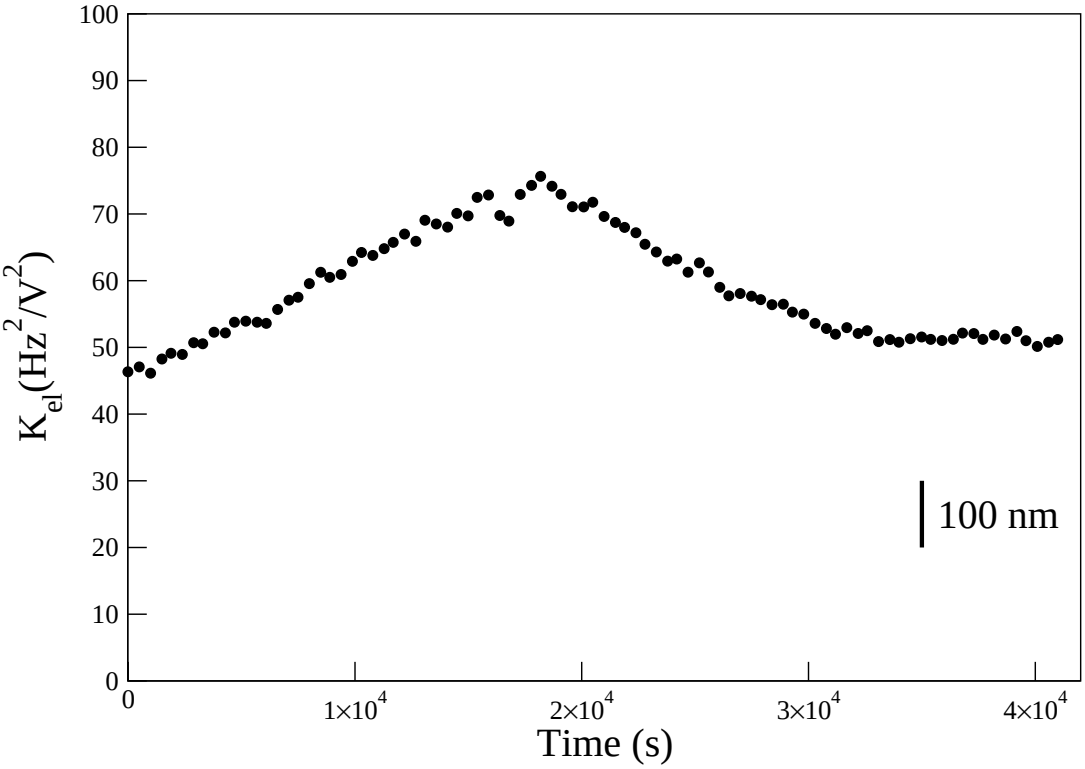

FIG. 8: Long-term drift of the curvature coefficient $K_{\rm el}$ during a 12 hours test. The vertical bar represents the equivalent drift in terms of the change in the sphere-plane separation, in the conservative hypothesis that all the drift is attributable to the gap drift. Subtracting each point with a window average of 4 measurements one gets a relative error in $K_{\rm el}$ of 4 %. The sensitivity to the choice of the average window time has been also assessed, with relative errors of 2.9 %, 4.1 %, 4.4 % and 4.6 % for alternative choices of 2, 6, 8, and 10 measurements, respectively.

Hence, the static deflection should play little role.

B. Thermal drift

Even though the temperature of the cantilever is actively stabilized by a Peltier cooler, the rest of the system is still subject to global thermal variation. In order to see this, we have measured $k_{\rm el}$ with respect to time at a nominally fixed distance. In the worst circumstance, the gap separation during the course of measurements can drift as much as 200 nm in *either* direction. Although such a drift could in principle affect the inferred exponent, a highly unlikely non-linear monotonic drift would be necessary to account for the consistently observed anomaly in each independent run.

C. Nonlinearity of the PZT actuation

The linearity of the PZT translation has been tested under a number of different circumstances. Notice that the translation intervals between the data points in each of the runs shown in are completely random. Yet, all of the runs obey a specific power law in all distances. The PZT was also independently calibrated by means of the fiber optic interferometer with a consistent, linear actuation coefficient factor $\beta = 87 \pm 2$ nm/V. Also, the presence of significant nonlinearities should manifest also as deviations from the PFA fitting of the sphere-plane capacitance versus the PZT voltage. As visible in Fig. 6, this class of measurements strongly constraint the PZT nonlinearity.

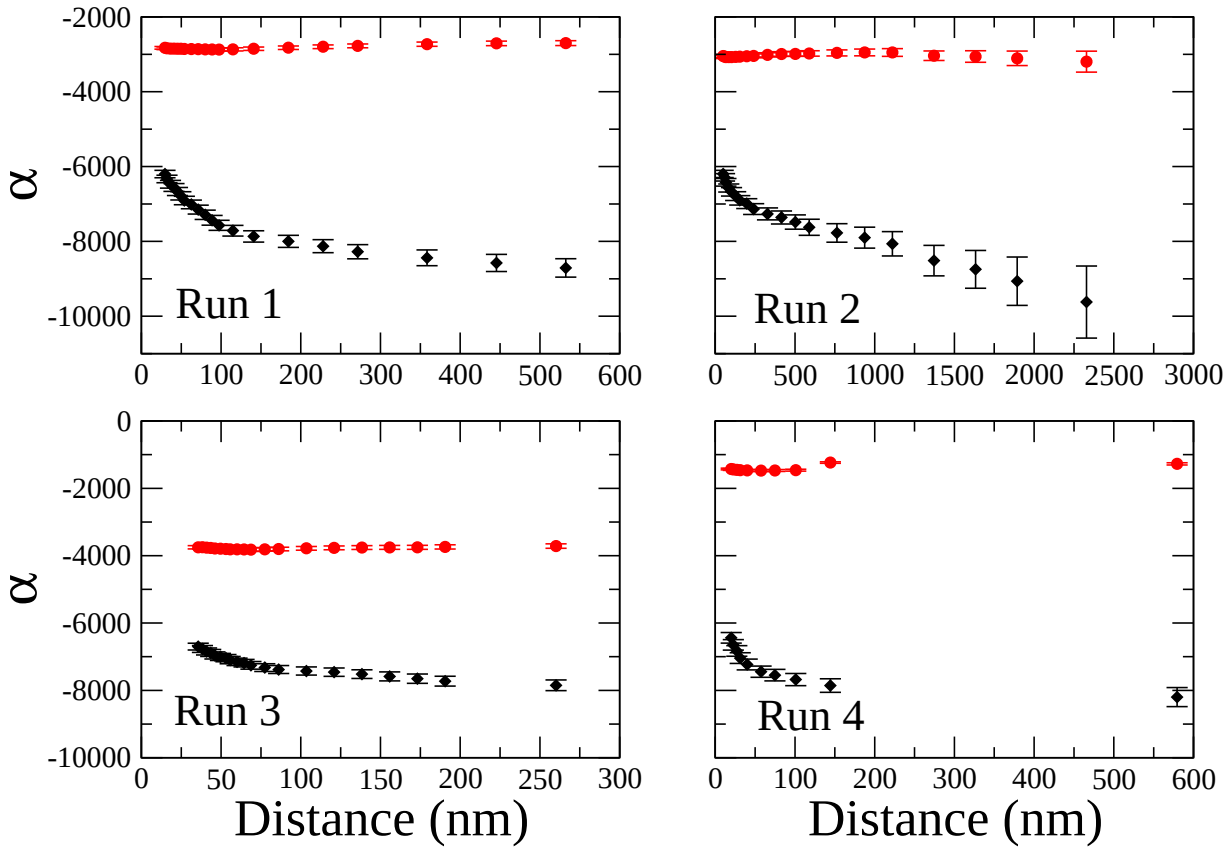

FIG. 9: Test of stability of the fit of the electrostatic calibrations: shown is the determination from the fitting of the calibration factor α in the case of the fixed -2 exponent versus the sphere-plane distance for the fixed -2 exponent (in units of Hz^2 V^{-2} m^2) expected from electrostatics (diamond points, black), and for the best exponent left as a free parameter (circle points, red). The number of points used in the data fit includes up to the gap distance evaluated at that point. The best exponent points show convergence to a constant value at the closest distances in all four runs, unlike the electrostatic case with the fixed exponent.

D. Nonlinear oscillation of cantilever

The cantilever is driven at resonance in a phase-locked loop, a routine technique adopted by many groups [18, 25, 49, 50]. Higher order terms in the force expansion should produce higher harmonics of the drive frequency. Then the assumption that the frequency shift is simply proportional to the gradient of the external force could lead to erroneous assessments of $k_{\rm el}$, eventually affecting the exponent. We have not observed higher harmonics in the frequency spectrum of the resonator.

E. Deviation from geometrical ideality

The deviation from geometrical ideality and its influence on the local capacitances [51] could in principle play a role, both in having a different shape or a variable radius of curvature, and in the deviations from the PFA formula. In our case, even at the smallest explored distances, the PFA correction due to the roughness is estimated to be of 0.4% in the electrostatic calibration, well below our sensitivity. A more careful analysis beyond the PFA is possible taking into account the actual surface profiles. It is however worth to point out that at least the simple hypothesis of a non uniform radius of curvature of the spherical surface cannot take into account the anomalous scaling. In PFA,

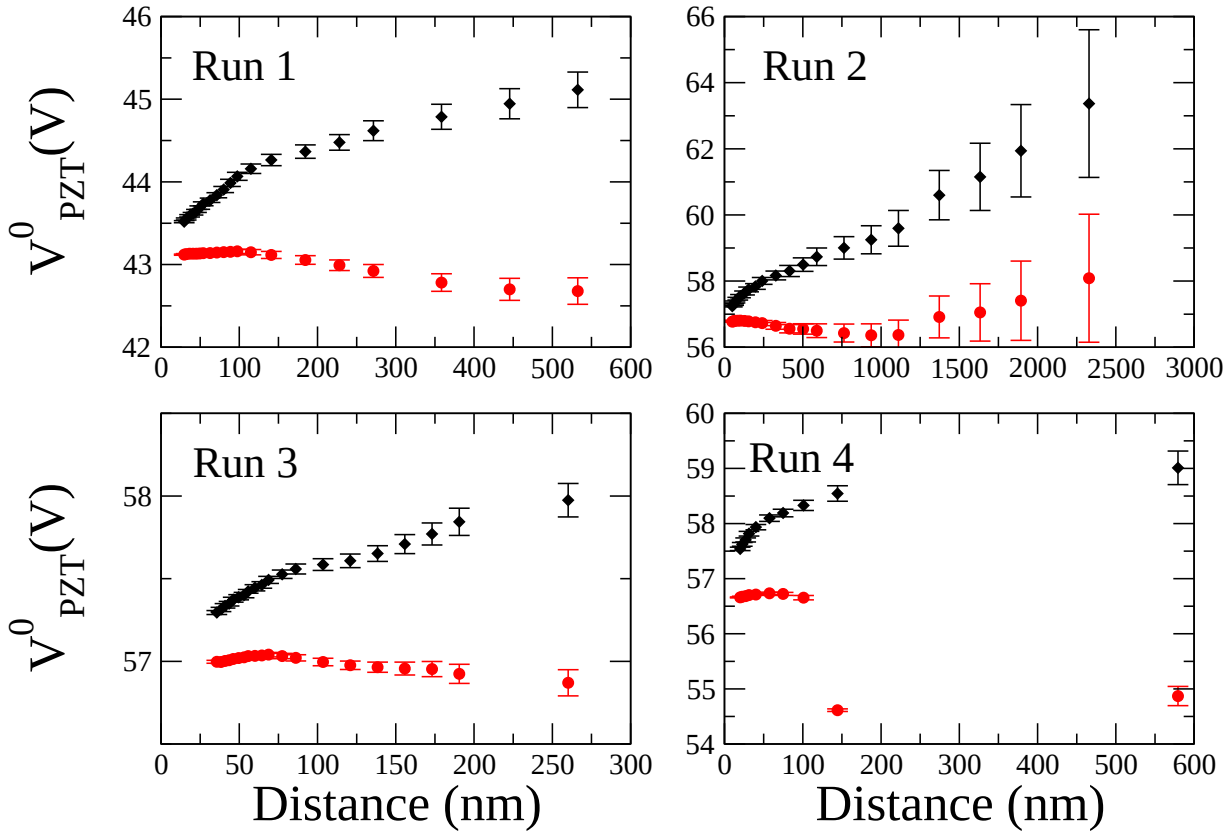

FIG. 10: Test of stability of the fit of the electrostatic calibrations: shown is the determination from the fitting of the offset distance $x_0 = \beta V^0_{\rm PZT}$ versus the sphere- plane distance in the case of the fixed -2 exponent expected from electrostatics (diamond points, black), and for the best exponent left as a free parameter (circle points, red). Clearly, the trend associated with the fixed exponent displays a wide variation in the fitting parameter $V^0_{\rm PZT}$, while the overall behavior driven by the best exponent shows a degree of stability in all distances.

the force signal (for both electrostatic and Casimir) is directly proportional to the radius of curvature and the total force will be therefore obtained as an integral along the radii of curvature with no deformations to the inverse square law for the distance dependence. In [52] an interesting geometry has been discussed which could take into account the anomalous exponent we have observed, however the stringent agreement between the capacitance measurements and the PFA expression for a pure sphere-plane geometry rules out this hypothesis.

F. Surface roughness

Roughness corrections become important at small separations between the surfaces, both for electrostatic calibrations and for analyzing their residuals in the search for Casimir forces. Usually roughness corrections in the electrostatic calibration are disregarded as such calibrations are performed at large distances. Here we consider the simplest analysis based on the proximity force approximation. Let us assume that both surfaces have stochastic roughness with rms amplitudes $\langle h_s^2 \rangle$ and $\langle h_p^2 \rangle$ for the sphere and plane respectively. Apart from the usual PFA condition to treat the curvature effects due to the spherical lens ($d \ll R$), we further assume that the sphere-plane distance d is much smaller than the lateral roughness correlation length ξ on each surface (this is the condition for the applicability of PFA to roughness considerations, only valid for very smooth surfaces). Further assuming that the rms roughness amplitudes are the smallest lengthscales in the problem, the PFA second-order perturbation correction to the sphere-plane electrostatic force is

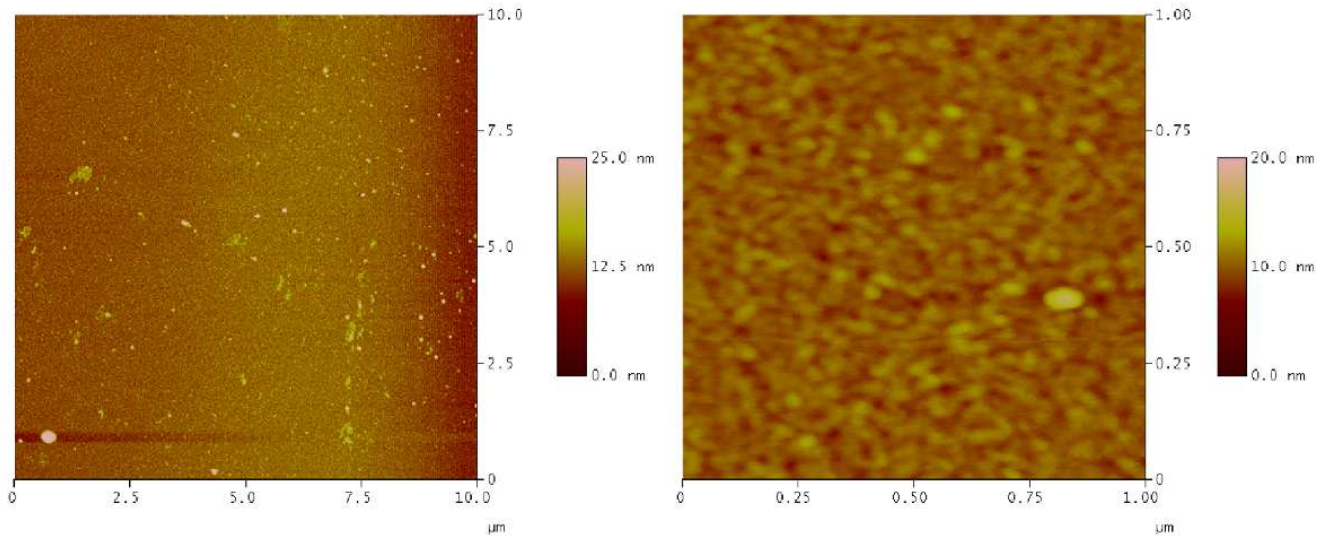

FIG. 11: Atomic force microscopy images of the cantilever surfaces, of size 10×10 μm (left) and 1×1 μm (right). The overall rms roughness for the larger surface is 1.54 nm (with a peak in the profile due to dust of 4.78 nm) and for the smaller surface is 0.79 nm (with a peak in the profile of 2.2 nm).

$$F_{\rm el}(x) = F_0(x)\left(1 + \frac{\langle h_s^2\rangle}{x^2} + \frac{\langle h_p^2\rangle}{x^2}\right), \tag{11}$$

where F_0 is the same force evaluated for smooth surfaces. Figure 11 shows typical images of the cantilever surface taken using AFM microscopy. We measured the surface profile for our surfaces and estimate the rms roughness of $\langle h_s^2\rangle = 4$ nm^2 and $\langle h_p^2\rangle = 2.4$ nm^2. The resulting deviation from ideality is below the estimated sensitivity of the apparatus, and an attempt to fit the electrostatic calibrations including the roughness at the PFA level as in Eq. 11 did result in significantly larger reduced χ^2. Roughness corrections to the electrostatic calibration potentially represent a systematic effect that could influence the residuals in the search of the Casimir contribution.

G. Patch potentials

Patch effects are expected to induce deviations from the Coulombian scaling with distance [37], and the fact that we have found in some calibrations a distance dependent minimizing potential could validate this hypothesis. However, this does not explain yet while the anomalous exponent is systematically observed in all runs, while only in some of them a manifest distance-dependent minimizing potential occurs.

IV. ANALYSIS OF THE RESIDUALS OF THE ELECTROSTATIC CALIBRATIONS AND TESTS OF THE CASIMIR FORCE

In the previous section we have found that the electrostatic calibrations performed in the entire measurement range show the presence of a distance-dependent minimizing potential (and therefore a distance-dependent contact potential) and an apparent deviation from the expectation for the sphere-plane capacitance dependence on distance. While the first systematic effect can be taken into account in the data analysis, the anomalous distance scaling of the electric force and the lack of its complete characterization prevents in principle to master the calibrations. This prevents the reliable determination of the relevant parameters of the system, for instance its effective mass, and

therefore the derivation of the residuals containing the Casimir force signal. In the absence of a complete analysis, and waiting for further experimental and theoretical input on the anomalous exponent observed in our configuration, in this section we analyze the cantilever square frequency $\nu_0^2(x)$ obtained by subtracting to the electrostatic calibration data the Coulombian electrostatic contribution based on the fitting procedure, as first performed in [45]. This off-line procedure is necessary as we have evidenced a dependence on distance of V_0 in various runs, and therefore we cannot assume *a priori* a unique counterbias voltage for an on-line subtraction of the residual electrostatic force as typically performed in various experiments. A distance-dependent residual frequency shift implies the presence of a non-Coulombian force or drifts in the intrinsic resonator frequency or a combination of both. It is evident in Eq. 8 that the electrostatic residual, $\Delta\nu_e^2(x, V_0)$, is zero only if the contact potential is constant. This term must be evaluated by first inferring the contact potential V_c through numerical integration of the minimum condition V_0.

Based on Eq. 7 we have a second order differential equation for $V_c(x)$:

$$\frac{C}{C''}\frac{d^2V_c(x)}{dx^2} + 2\frac{C'}{C''}\frac{dV_c}{dx} + V_c(x) = V_0(x), \tag{12}$$

where $V_0(x)$ is determined experimentally. For the sphere-plane case in the PFA this results in the following differential equation:

$$x^2\ln(R/x)\frac{d^2V_c(x)}{dx^2} - 2x\frac{dV_c(x)}{dx} + V_c(x) = V_0(x). \tag{13}$$

to be solved numerically for instance using a Runge-Kutta integration method, once the experimental data on $V_0(x)$ are interpolated with an analytic function. In the absence of a model for the dependence on distance of V_0, different equivalent empirical functions can be used to fit the actual data. This obviously is a strong limitation to the predictive power on the residuals, but at a phenomenological level has to be considered as a conservative and realistic procedure to infer some physics beyond the Coulombian contribution. We use, as first guess function, an exponential one such as $V_0(x) = V_0 + \Delta V[1-\exp(-x/\lambda)]$ with V_0 representing the potential when the two surfaces are in contact, $V_0 + \Delta V$ is the asymptotic value of the minimizing potential at large distances, and λ the characteristic lengthscale on which the minimizing potential varies. Alternatively, we may use the function $V_0(x) = V_{\log} + \Delta V_{\log}\ln(x/\Lambda)$, characterized by similar parameters $V_{\log}$, $\Delta V_{\log}$ and Λ, although in this case a defined asymptotic value is not available. In Fig. 12 we show the sensitivity of V_c obtained through integration of Eq. 13 to the choice of the function interpolating the V_0 distance dependence.

Another issue requiring careful attention regards the boundary conditions chosen to solve the second order differential equation for $V_c(x)$. At large distances $V_c(x)$ is expected to be constant and thus $V_c(x) = V_0(x)$. Also, the first derivative of $V_c(x)$ should be zero in order to satisfy the differential equation. Therefore we choose the boundary condition $V_c(x_n) = V_0(x_n); V_c'(x_n) = 0$, where x_n is the largest distance measured in the data set. In the case of the exponential fitting of $V_0(x)$, the curve becomes quickly flat as x increases and therefore the use of x_n at very large distances is a good approximation. For the logarithmic fitting this is more problematic, making the solution for $V_c(x)$ quite sensitive to the choice of x_n.

Based on this input, one can evaluate now the electrostatic contribution independent on the external bias potential, $\Delta\nu_e^2(x, V_0)$, and further subtract it from electrostatic contribution dependent on the external bias evaluate at the minimizing potential, $\nu_m^2(x, V = V_0)$ (*i.e.*, the maximum of each parabola in Fig. 3). The result is shown in Fig. 13, where the dashed and dotted-dashed curves are relative to the choice of the V_0 dependence on distance, as given in Fig. 12 (either exponential or logarithmic). We see that the plotted quantities $\nu_m^2(x, V = V_0) - \Delta\nu_e^2(x, V_0)$ indicate that there are further distance-dependent residuals $\nu_p^2 + \Delta\nu^2(x)$ of non-electrostatic nature. In this analysis it is critical to have the most accurate control on the dependence of V_0 on distance. In case of runs 2, 3, and 4 such a control is quite limited, and neither an exponential function nor a logarithmic function adequately describe its spatial dependence. In the remainder of this section we will concentrate on run 1.

Given the serious limitations of our electrostatic calibration, it is difficult to perform a rigorousanalysis of these extra residuals, as they could be Casimir-Lifshitz forces, patch potential forces,etc. In the following we will *assume* that these extra residuals are only due to the Casimir-Lifshitz force, and evaluate the corresponding prediction for $\nu_p^2 + \Delta\nu_{\rm Cas}^2(x)$. As a first attempt, one can fit either the exponential (dashed line) or the logarithmic (dotted-dashed line) residuals in Fig. 13 with the plain Casimir formula for zero temperature and perfect metals. In the proximity force approximation,the sphere-plane Casimir force is $F_{\rm Cas}(x) = 2\pi R E_{\rm PP}(x)$, where $E_{\rm PP}(x)$ is the Casimir energy per unit area for the plane-plane configuration, $E_{\rm PP}(x) = -\hbar c\pi^2/720x^3$. Therefore, the frequency shift due to the Casimir force in the sphere-plane case is $\Delta\nu_{\rm Cas}^2(x) = -K_{\rm Cas}/x^4$, with $K_{\rm Cas} = \pi\hbar cR/480m_{\rm eff}$. Fitting the above curves with $\nu_p^2 - K_{\rm Cas}/x^4$, we obtain $\nu_p^2 = (790440 \pm 19.3)\mathrm{Hz}^2$, $K_{\rm Cas} = (5.5164 \pm 0.3390) \times 10^{-27}\mathrm{Hz}^2/\mathrm{m}^4$ for the dashed line (exponential formula for $V_0(x)$), and $\nu_p^2 = (790450 \pm 18.3)\mathrm{Hz}^2$, $K_{\rm Cas} = (6.5795 \pm 0.3220) \times 10^{-27}\mathrm{Hz}^2/\mathrm{m}^4$ for

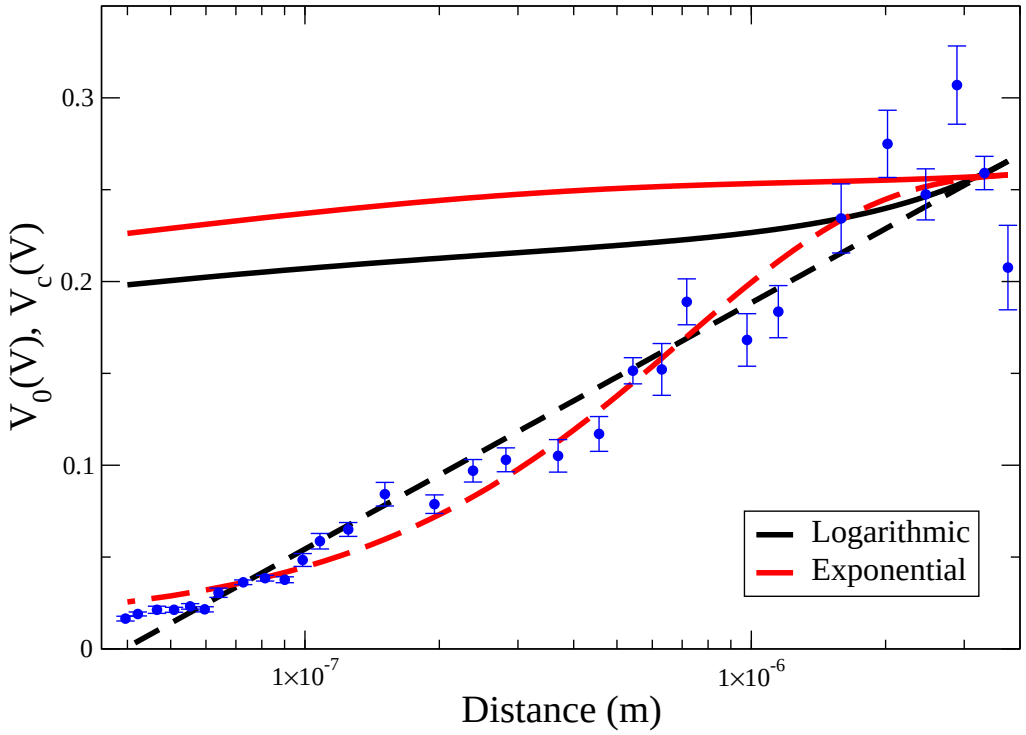

FIG. 12: Data for the minimizing potential V_0 versus sphere-plane distance for run 1. The dashed curves represent the best fits of V_0 assuming an exponential dependence (red) and a logarithmic dependence (black). The best fit parameters are $V_0 = (0.011 \pm 0.007)$V, $\Delta V = (0.25 \pm 0.01)$V, and $\lambda = (703 \pm 93)$ nm in the case of the exponential function, and $V_{\rm log} = (0.07 \pm 1140)$ V, $\Delta V_{\rm log} = (0.058 \pm 0.003)$ V, and $\Lambda = (140.4 \pm 2.8)$ nm in the case of the logarithmic function. The continuous curves represent the corresponding plots of the contact potential V_c after solving the differential equation Eq. 13 as described in the text.

the dashed-dotted line (logarithmic formula for $V_0(x)$). Using the values for the radius of curvature of the sphere of $R = 30.9$mm, and an effective mass of $m_{\rm eff} = 0.46$g, the obtained coefficients $K_{\rm Cas}$ are lower than theideal Casimir prediction ($K_{\rm Cas,th} = 1.3\times10^{-26}{\rm Hz}^2/{\rm m}^4$)by about a factor 2,in line with the expectation that conductivity corrections could play a role.

In order to analyze possible conductivity (and temperature) corrections to the Casimir force we now use the Lifshitz formalism [53], written in terms of the frequency-dependent reflection coefficients of the two gold surfaces. The plane-plane free energy is

$$E_{\rm PP}(x) = \frac{k_B T}{2\pi x^2} \sum_p {\sum_{m=0}}' \int_{m\gamma}^{\infty} dy\; y^2\; \log(1 - r_p^2\; e^{-2y}). \tag{14}$$

Here p denotes the two possible polarizations (TE and TM), $\gamma = 2\pi k_B T x/\hbar c$, and the prime on the summation sign indicates that the $m = 0$ term is counted with half weight. The reflection amplitudes are given by the usual Fresnel formulas,

$$r_{\rm TM}(y,\xi_m) = \frac{s_m - \epsilon(i\xi_m)p_m}{s_m + \epsilon(i\xi_m)p_m} \;\; ; \;\; r_{\rm TE}(y,\xi_m) = -\frac{s_m - p_m}{s_m + p_m}, \tag{15}$$

where $\xi_m = 2\pi k_B T m/\hbar$ are the Matsubara frequencies, $p_m = y/m\gamma$, and $s_m = \sqrt{\epsilon(i\xi_m) - 1 + p_m^2}$. The dielectric permittivity at imaginary frequencies is evaluated using Kramers-Kronig relations with gold optical data from Palik [54], extrapolated to low frequencies using a Drude model with parameters: $\omega_p = 7.5$eV for the plasma frequency, and $\gamma_p = 0.061$eV for the plasma relaxation parameter. The resulting theoretical prediction (using once again PFA for the

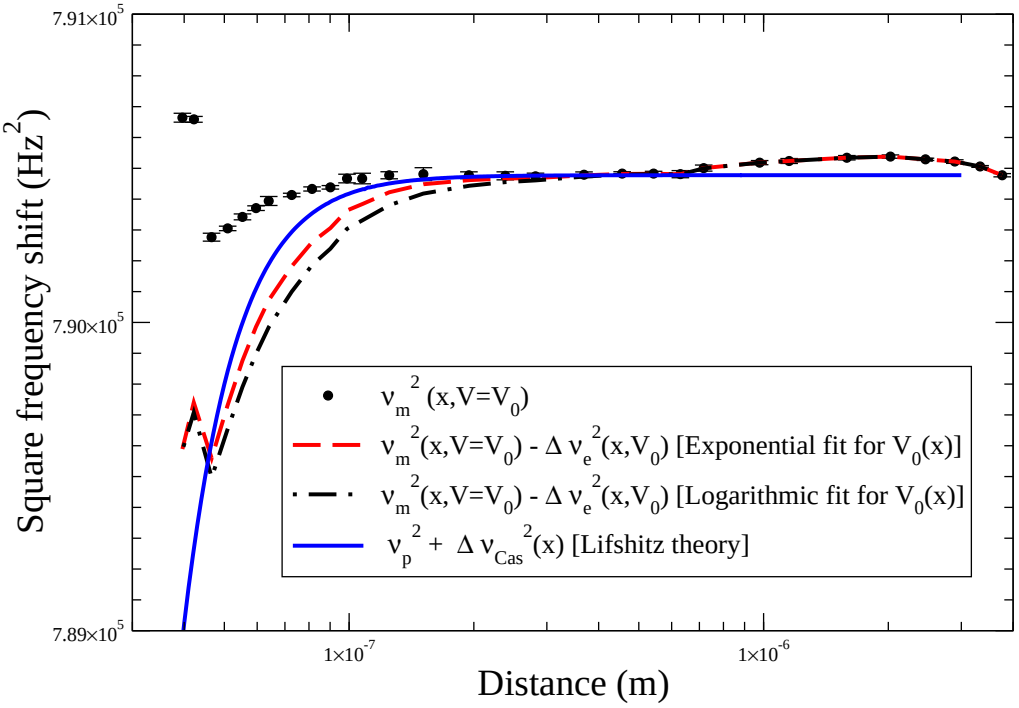

FIG. 13: Plot of the electrostatic residuals versus distance. The dots correspond to the maximum value of each parabola in Fig. 3 as a function of distance, $\nu_m^2(x, V = V_0)$. The dashed (exponential fit for $V_0(x)$) and dotted-dashed (logarithmic fit for $V_0(x)$) lines result from substracting from $\nu_m^2(x, V = V_0)$ the extra term $\Delta\nu_e^2(x, V_0)$ due to the distance-dependence of the contact potential $V_c(x)$. The dotted line is the Lifshitz prediction for $\nu_p^2 + \Delta\nu_{\rm Cas}^2(x)$. Parameters are an effective mass $m_{\rm eff}$ =0.46 g and a cantilever free oscillation frequency $\nu_p = 889.09$Hz. Optical data of gold are from Palik [54], and Drude parameters are $\omega_p = 7.5$eV and$\gamma = 0.061$eV. Temperature is set to $T = 300$K.

sphere-plane case) for $\nu_p^2 + \Delta\nu_{\rm Cas}^2(x)$ at $T = 300$K is plotted as the dotted line in Fig. 13, using as the free cantilever square frequency $\nu_p^2 = 7.9047767 \times 10^5$ Hz^2. It is apparent from the figure that the Casimir curve $\nu_p^2 + \Delta\nu_{\rm Cas}^2(x)$ approximately follows the behavior of the curves $\nu_m^2(x, V = V_0) - \Delta\nu_e^2(x, V_0)$ (that is, the electrostatic residuals *after* substraction of the distance-dependent contact potential term). Note that $\Delta\nu_e^2(x, V_0) > 0$, that means a positive frequency shift associated to a *repulsive* electrostatic residual (V-independent) force. Had we not taken this term into account, the Lifshitz theory curve would noticeably depart from the electrostatic residuals $\nu_m^2(x, V = V_0)$.

Finally, it is important to emphasize once again that, due to the anomalous exponentwe found in our electrostatic calibration, we cannot make any precision measurement claims on the Casimir force after the residual analysis. Nor does our data have enough sensitivity to detect corrections due to temperature effects or sample dependence. On the other hand, it is quite possible that part of the residuals are due not only to Casimir-like forcesbut also to other external voltage-independent forces, not taken into account in a simple Coulomb law, such as patch potentials.

V. SYSTEMATIC EFFECTS AND RELATIONSHIP TO PREVIOUS CASIMIR AND AFM EXPERIMENTS

Our experiment spans between two different classes of experiments. In previous short-distance Casimir force experiments, the minimum explored distance is on the order of few hundred nanometers. This is due to the fact that typically, in order to increase the sensitivity at larger distances, the stiffness of the resonator is designed to be low. While this yields a stronger signal at large distances with respect to harder resonators, this also results in an earlier snapping of the resonator to the attracting surface. On the other hand, typical AFM experiments aimed at mapping the profile of a surface at subnanometer resolution (both depth and lateral) do not need to reach distances larger than 10-20 nm. We discuss here more in general the specific issues we have found that could affect at least in

principle the analysis of previous measurements, or at least the assessment of their accuracy.

A. Distance dependence of the contact potential

Our finding of the dependence of the contact potential V_c upon the distance calls for a more careful study of previous experiments in which the contact potential was assessed at relatively larger gaps than the one used for looking at the Casimir force. In order to seek for similar regularities in previous Casimir force experiments, we have requested electrostatic calibration data kindly provided by various groups. The result of the analysis for the data of the Lucent Laboratories group [17] working with spheres of much smaller radius of curvature (100 μm) is reported in the top-right plot in Fig. 14, showing a small but clearly visible linear correlation between V_0 and the sphere-plane distance. The data of the AFM group in Grenoble (with microspheres of radius 20 μm) in Fig. 14 bottom-left show also a strong dependence of V_0 at large distances, with a more complex behavior as evident from the change in polarity of the minimizing potential around 5 μm. In the case of the experiment performed at Indiana University-Purdue University Indianapolis (IUPUI), with a microsphere of radius (148.7 ± 0.2) μm, see bottom-right plot, no evident dependence on the distance can be assessed, and in that experiment a constant counterbias equal to the average value was assumed. A linear trend, with a systematic difference in the contact potential in the explored range of about 3 mV around random fluctuations of comparable size, seems also present in Fig. 4 of [55] using microspheres of radius 200 μm, although the coarse scale used for the vertical units makes harder a more careful and quantitative assessment.

Although it would be necessary to collect more data, one noticeable emerging pattern from the comparison of the experiments in Fig. 14 is that experiments with intermediate radii of curvature generally seem to provide a milder dependence of V_0 within a comparable distance range. It is plausible that spheres with very small radius of curvature as in the example from the Grenoble group are more vulnerable to local defects or impurities, while large radii of curvature (and therefore large active interaction surfaces) like in our case are sensitive to large scale variations in the patch potentials. It will be interesting to investigate, beside the obvious material composition, the geometry dependence of minimizing and contact potentials. An interesting study of the minimizing potential and its dependence upon distance and drift in time has been recently reported for the more macroscopic setup of a torsional balance [56].

To assess the impact of the distance-dependent minimizing potential on the precision of the Casimir force measurements, following [57], we evaluate the equivalent voltage necessary to mimic the ideal (zero temperature, perfect conductors) Casimir force at a given distance, and in the sphere-plane case we have

$$V_{\rm eq}(x) = \frac{\pi}{120}\left(\frac{\hbar c}{\epsilon_0}\right)^{1/2}\frac{1}{x}, \tag{16}$$

implying that the Casimir force can be simulated, at a distance of 1 μm, by just having 17.5 mV of uncompensated voltage between the two surfaces. For real materials the Casimir force is weaker, and can therefore be mimicked by an even smaller uncompensated voltage. If the minimizing potential V_0 is independent of the distance over the entire range of explored distances, it is legitimate to use an external counterbias to cancel its effect. Otherwise, a fixed counterbias will only cancel out the minimizing potential at a given distance and, depending on the slope of V_0 versus distance at smaller gaps, most if not all of the measured force could be due to the uncompensated potential. Some of the determinations of the contact potential in previous experiments have been performed at relatively large gaps with respect to those at which the Casimir forces observations are reported. In some cases, in particular for low stiffness microcantilevers, this is necessary because electrostatic forces at small distances will cause snapping or instabilities, unless very small bias voltages, limited by the voltage supply specifics, are applied. This suggests that a reanalysis of the data collected on Casimir forces so far will be beneficial in the light of these findings, also including a more careful scrutiny in the next round of measurements. Notice also that to have for instance a 0.1 % precision in the determination of the Casimir force the electrostatic background should be controlled with an accuracy better than 550 μV at 1 μm, which it is also equivalent to perform precision electrometry. In other words, the precision of 0.1 % is equivalent to be able to discern a minimum voltage of 550 μV applied to the gap, a very difficult task considering the presence of comparable voltage drifts and patch potentials, although other groups have instead concluded that the estimated patch potential contributions are under control in their experiments [23, 58].

B. Thermal expansion

Even though the temperature of the cantilever clamping system is actively stabilized by a Peltier cooler, the rest of the system is still subject to global thermal variation as large as 1 K during the measurement runs. In order to understand the stability issues of our apparatus, we have studied the cantilever frequency for a time interval much

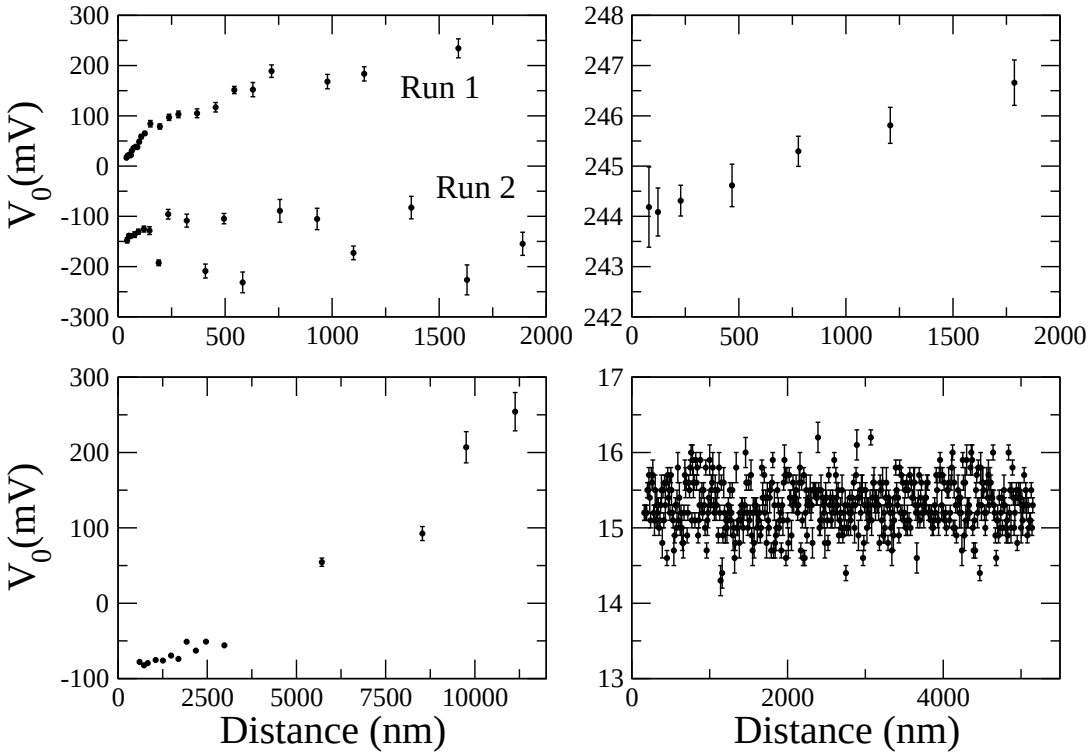

FIG. 14: Minimizing voltage versus sphere-cantilever distance resulting for the data analysis of various experiments. Shown are data from run 1 and run 2 of our experiment (top-left, with a zero minimizing potential at the closest approach for run 1, and a non-zero value of $V_0 \simeq$-150 mV for the closest approach of run 2), data from [17] (top-right, courtesy of F. Capasso and H.B. Chan), results from the experiment of the Grenoble group (bottom-left, courtesy of J. Chevrier and G. Jourdan) , and the experiment at IUPUI (bottom-right, courtesy of R. Decca). The first three sets of data evidence a distance dependence of V_0 upon the sphere-plane separation, which could affect significantly the accuracy without taking into account this systematic effect, while this behaviour is absent in the bottom-right plot.

longer (12 hours) than the typical duration of a run (of 3-4 hours) and we have show the temporal evolution of the curvature coefficient $K_{\rm el}$ at a given nominal distance in Fig. 8.

To understand the impact of thermal expansions let us consider an aluminum slab of L =1 cm with its coefficient of linear expansion $\alpha = 24 \times 10^{-6}$/K, situated underneath the cantilever. For a typical temperature change over a period of 12 hours of $\Delta T = 1$K, the incremental expansion due to temperature is then $\Delta L = \alpha L \Delta T$ =240 nm, which is almost identical as the total distance variation shown in Fig. 8. This translates into a range of 5-10 nm of average variation in the shot-to-shot electrostatic measurement, *i.e.* the change in the absolute gap separation during the acquisition of an individual data point. To evaluate the robustness of the fits, let us assume that the last position registered by the PZT right before hard contact is misplaced by 8 nm either closer or away from the surface, for instance due to thermal expansion. One underlying assumption held throughout our analysis has been the distance measurement is solely controlled by the action of the piezoelectric transducer, but it is evident at this point that the actual distances could be also affected by thermal expansion. In order to see how this small variation due to temperature change influences the final results of the fitting procedure, we have adjusted the last data point of the closest approach by 8 nm forward or backward in an attempt to mimic the effect of a thermal expansion hypothetically affecting only the last collected point.

The relocation of the single data point of the final distance has modified the entire set of fitting parameters as shown in Table 2. For the case of the calibration factor α, variations due to the modification of the single last data point were $14\%, 6.4\%, 18\%, 21\%$ for Run 1-4, respectively. Even larger changes in the values of the distance offset x_0 were found, up to 40 %.

The exponent e of the electrostatic power law, however, remains stable over the forward and backward displacements

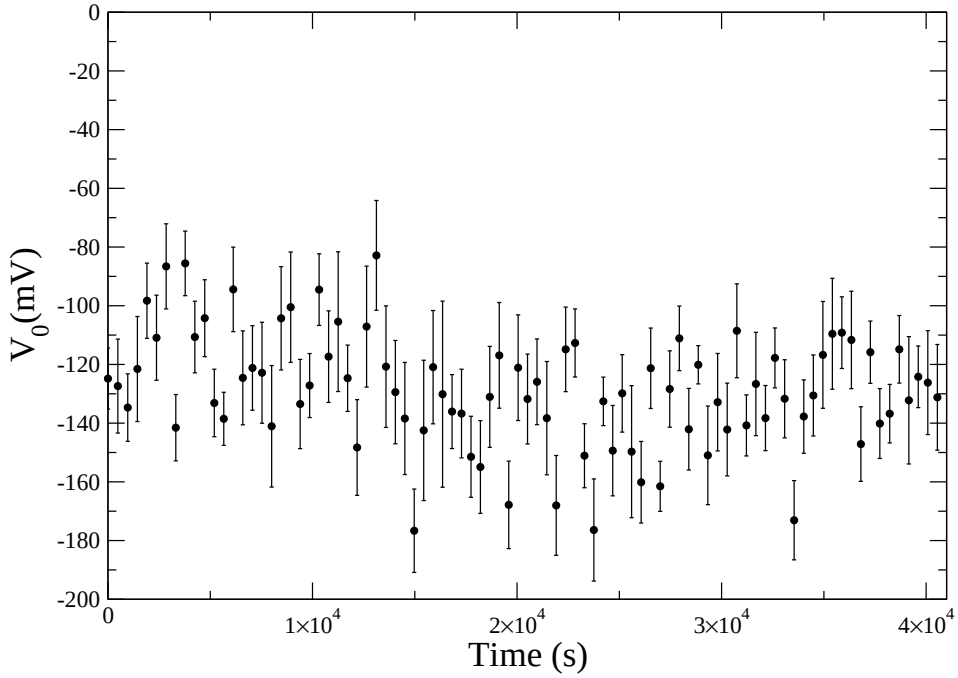

FIG. 15: Time behaviour of V_0 in the same long run of Fig. 8. The apparent lack of correlation between this drift and the one presented in Fig. 8, which is mainly due to the drift in the sphere-plane gap distance, seems to imply that there are genuine time-dependent drifts of the minimizing potential even if the sphere-plane distance is kept constant, consistently with the finding in [56].

of the single data point, although its overall variation is evidently greater than the fitting uncertainties at a given position, demonstrating how vulnerable fitting parameters are to small changes in the absolute gap distance. It should be emphasized that only a single data point is readjusted in this analysis. Because the thermal expansion is present throughout the whole measurement at all distances, what has been shown here only represents a subset of many other possibilities.

Another source of drift has been identified in the minimizing potential, as evidenced in Fig. 15. This is consistent with recent reports of dedicated experiments studying the long term drift of the surface potential using torsional

		Run 1	Run 2	Run 3	Run 4
F	$\alpha(\mathrm{Hz^2V^{-2}m^e})$	3194 ± 97	3200 ± 158	4265 ± 155	1749 ± 75
	x_0 (nm)	35.7 ± 0.1	53.9 ± 0.3	43.5 ± 0.2	28.7 ± 0.2
	e	-1.74 ± 0.01	-1.78 ± 0.02	-1.84 ± 0.01	-1.60 ± 0.01
	χ^2/DOF	1.6	0.5	2.2	7.0
	$\alpha(\mathrm{Hz^2V^{-2}m^e})$	2805 ± 92	3021 ± 153	3732 ± 144	1415 ± 69
	x_0 (nm)	29.6 ± 0.1	49.6 ± 0.2	35.7 ± 0.2	20.0 ± 0.2
	e	-1.70 ± 0.01	-1.77 ± 0.02	-1.80 ± 0.01	-1.54 ± 0.02
	χ^2/DOF	1.0	0.8	1.2	7.0
B	$\alpha(\mathrm{Hz^2V^{-2}m^e})$	2788 ± 97	3006 ± 162	3608 ± 149	1451 ± 78
	x_0(nm)	28.7 ± 0.2	48.7 ± 0.3	33.9 ± 0.2	20.0 ± 0.2
	e	-1.70 ± 0.01	-1.77 ± 0.02	-1.79 ± 0.01	-1.54 ± 0.02
	χ^2/DOF	2.8	1.6	1.7	11.5

TABLE II: Stability test of the fitting parameters for the electrostatic calibrations. The middle rows present the fitting parameters α and x_0 for the electrostatic calibrations with a power law exponent e taken to be a free parameter, such that $K_{el} \propto d^e$. F and B in the first and third rows represent hypothetical situations in which the last data point right before hard contact were moved by 8 nm forward (F) and backward (B) from the original position, respectively.

balances [56]. The presence of a minimizing potential slowly drifting in time implies severe limitations on the possibility to integrate for long time intervals precision force measurements.

C. Relationship between Casimir and AFM measurements

For the sphere-plane geometry, Casimir force experiments have used sphere radii much larger than typical in AFM apparatus ($R \simeq 100\mu$m versus 10-100 nm respectively) due to different motivations (mesoscopic effective surface versus higher image resolution, respectively). However, the physics ruling the instrument should be the same and one expects a smooth transition between the two regimes, and a close comparison between the accuracies reachable in these two regimes. Many of the systematic effects that can potentially mimic the Casimir force have been extensively studied in the AFM experiments [44, 50, 59], in particular for the investigation of adhesion and friction surface forces [60, 61, 62, 63], many years before Lamoreaux's landmark experiment [15]. Dürig *et al.* have studied metallic adhesion and short range forces using Scanning Tunneling Microscopy (STM) [64, 65], while a number of papers are devoted to the subject of radiative transfer [66], noncontact friction [67], and dissipative interaction between a resonant cantilever and various sample surfaces in the dynamic AFM mode [36, 68, 69, 70, 71, 72], still an active topic of research. It would be productive to bridge the short-range AFM measurements and Casimir force measurements that, after the pioneering measurements of the macroscopic van der Waals force [73], seem to have developed with somewhat divergent methodologies.

The Casimir force may be considered as the van der Waals force in the long-range, retarded regime and therefore the study of its nature may be seen as an extension of the general studies of the previous van der Waals force measurements with AFM techniques. From this perspective, the measurement of forces between macroscopic surfaces at small distances becomes a rich field of study, including also the possible role played by the meniscus force, double-layer force, capillary force, hydration force, hydrophobic force, and steric, depletion, and bridge forces, all ultimately of electromagnetic origin, yet different in distance scaling and strength [47]. Although not all of these forces may be relevant in a given experimental situation, one must carefully check the presence of each of these forces and must be able to distinguish them, on the top of residual electrostatic forces and Casimir forces in themselves. It is plausible that, especially at the level of accuracy reachable in current and future high precision measurements of the Casimir force at small distances, some of these forces should appear already at the level of residuals from the best fits.

A similar argument may be also applied to the electrostatic calibrations. The AFM community has already discussed issues such as friction, electrification, patch charges and potentials, while these have received little attention so far in the Casimir framework (apart from the estimates for the effect of the patch potentials discussed in [23, 58]), in spite of relevant analysis appearing in the recent literature [37, 74, 75]. Also, Burnham *et al.* [63] have evaluated the effect of patch charges by means of the image method, and compared with the previously observed long-range interaction of van der Waals force in the surface force microscopy. In [36], the force fluctuations between a cantilever tip ($R = 1\mu$m) and a surface (both gold-coated) are interpreted in terms of inhomogeneous electric fields due to the presence of atomic steps, adsorbates, hillocks, pits, and other defects. The ubiquity of these electric fields may significantly limit precision and accuracy of Casimir force measurements. It is therefore of great relevance to aim also at calibrations with other physical effects, such as through radiation pressure [26] and hydrodynamic forces in the case of the Casimir-Lifshitz force in the presence of liquid media [76], and to perform detailed comparisons among the various calibration techniques, especially to filter out issues specific to the electrostatic calibrations.

VI. CONCLUSIONS

We have discussed electrostatic calibrations in a sphere-plane setup different from the previous ones for two features, namely a large radius of curvature of the sphere and a microresonator with large stiffness. This combination allows us to extend electrostatic calibrations to small gap distances in the presence of large spherical surfaces. We have evidenced anomalies in the expected scaling of the electrostatic force, and a distance dependent potential minimizing the electrostatic contribution. In the absence of a complete control of the underlying electrostatic physics, it is difficult to calibrate the apparatus at the extent to meaningfully discuss the residuals signal. By using the electrostatic expectations, we have found evidence of the Casimir-Lifshitz force at small separation in one out of the four runs for which optimal working conditions were found and a complete data analysis have been performed. While we believe that some systematic effects are being emphasized by using spheres with large radius of curvature and small sphere-plane distances, we draw two conclusions from our results which may be of more general interest. Firstly, we have shown that the determination at all distances of the contact potential V_0 is crucial, and its uncertainty can affect the entire data analysis procedure. This implies that electrostatic calibrations have to be performed in the entire range of explored distances, rather than being limited to larger separations for which the Casimir force is expected

to be negligible. Secondly, we have discussed the stability of the determination of the fit parameters, like distance offset, minimizing potential, and effective mass, coming from the electrostatic calibrations. Various groups are now trying to confirm or rule out the anomalies we have observed in our experimental setup [77]. Apart from pointing out some limitations of the sphere-plane geometry, we believe that our discussion of systematic effects and data fitting robustness is beneficial for more rigorous data analysis in the next generation of experiments for any geometrical configuration, allowing to explore non-Coulombian forces, in the spirit of an experiment able to discover unknown physics rather than the demonstration of an *a priori* known effect [31].

*Present address: Department of Physics, Yale University, 217 Prospect Street, New Haven, CT 06520-8120, USA

We thank R.L. Johnson for skillful technical support, and Q. Wei for experimental assistance. M.B.H. acknowledges support from the Dartmouth Graduate Fellowship program and the NSF GAAN program. W.J.K. acknowledges useful discussions with S.K. Lamoreaux and A. Parsegian, while D.A.R.D. acknowledges interesting discussions with G. Carugno, H.B. Chan, R. Decca, S. de Man, S.K. Lamoreaux, U. Mohideen, J. Munday, and G. Ruoso. R.O. acknowledges partial support by the NSF through the Institute for Theoretical Atomic and Molecular Physics at Harvard University and the Smithsonian Astrophysical Observatory, and is grateful to F. Capasso and H.B. Chan for kind permission to use a set of their electrostatic calibration data from [17] for the analysis reported in Fig. 14, to J. Chevrier and G. Jourdan for useful discussions and for providing data reported in Fig. 14 prior to their publication, and to R. Decca for useful discussions and for providing data of his experiment reported in Fig. 14.

[1] Casimir H B G 1948 *Proc. K. Ned. Akad. Wet.* B **51** 793
[2] Lifshitz E M 1956 *Zh. Eksp. Teor. Fiz* **29** 94 [*Sov. Phys. JETP* **2** 73]
[3] Plunien G, Müller B, and Greiner W 1986 *Phys. Rep.* **134** 87
[4] Milonni P W 1994 *T*he Quantum Vacuum (San Diego: Academic Press)
[5] Mostepanenko V M and Trunov N N 1997 *T*he Casimir Effect and its Applications (London: Clarendon)
[6] Bordag M 1999 *T*he Casimir Effect 50 Years Later (Singapore: World Scientific)
[7] Bordag M, Mohideen U, and Mostepanenko V M 2001 *Phys. Rep.* **353** 1
[8] Reynaud S, Lambrecht A, Genet C, and Jaekel M T 2001 *C. R. Acad. Sci. Paris* **IV-2** 1287
[9] Milton K A 2001 *T*he Casimir Effect: Physical Manifestations of the Zero-Point Energy (Singapore: World Scientific)
[10] Milton K A 2004 *J. Phys. A: Math. Gen.* **37** R209
[11] Lamoreaux S K 2005 *Rep. Prog. Phys.* **68** 201
[12] Sparnaay M J 1958 *Physica* **24** 751
[13] van Blokland P H G M and Oveerbeek J T G 1978 *J. Chem. Soc. Faraday Trans. I* **74** 2637
[14] Bressi G, Carugno G, Onofrio R, and Ruoso G 2002 *Phys. Rev. Lett.* **88** 041804
[15] Lamoreaux S K 1997 *Phys. Rev. Lett.* **78** 5
[16] Mohideen U and Roy A 1998 *Phys. Rev. Lett.* **81** 4549; Harris B W, Chen F, and Mohideen U 2000 *Phys. Rev. A* **62** 052109
[17] Chan H B, Aksyuk V A, Kleiman R N, Bishop D J, and Capasso F 2001 *Science* **291** 1941
[18] Decca R S, López D, Fischbach E, and Krause D E 2003 *Phys. Rev. Lett.* **91** 050402; Decca R S *et al.* 2005 *Phys. Rev. Lett.* **94** 240401
[19] Decca R S, López D, Fischbach E, Klimchitskaya G, Krause DE, Mostepanenko VM 2007 *Phys. Rev. D* **75** 077101; 2007 *Eur. Phys. J. C* **51**, 963
[20] Derjaguin B V and Abrikosova I I 1957 *Sov. Phys. JETP* **3** 819; Derjaguin B V 1960 *Sci. Am.* **203** 47
[21] Blocki J, Randrup J, Swiatecki W J, and Tsang F 1977 *Ann. Phys.* **105** 427
[22] Krause D E, Decca R S, López D, and Fischbach E 2007 *Phys. Rev. Lett.* **98** 050403
[23] Decca R S, López D, Fischbach E, Klimchitskaya G L, Krause D E, and Mostepanenko V M 2005 *Annals of Physics* **318** 37
[24] van Zwol P J, Palasantzas G, and de Hosson J Th M 2007 *Appl. Phys. Lett.* **91** 144108; 2008 *Phys. Rev. B* **77** 035439; 2008 *Phys. Rev. B* **77** 075412; van Zwol P J, Palasantzas G, van de Schootbrugge M, de Hosson J Th M, and Craig V S J 2008 *Langmuir* **24** 7528
[25] Jourdan G, Lambrecht A, Comin F, and Chevrier J 2007 arXiv:0712.1767v1 [physics.gen-ph] 11 Dec 2007
[26] Petrov V, Hahn J, Petter J, Petrov M, and Tschudi T 2005 *Optics Lett.* **30** 3138; Petrov V, Petrov M, Bryksin V, Petter J, and Tschudi T 2006 *Optics Lett.* **31** 3167; Bryksin V and Petrov M 2007 *JETP Letters* **86** 368; Bryksin V and Petrov M 2008 *Phys. Solid State* **50** 229
[27] Ludwig T 2008 *J. Phys. A* **41** 164025
[28] Chan H B, Bao Y, Zou J, Cirelli R A, Klemens F, Mansfield W M, and Pai C S 2008 *Phys. Rev. Lett.* **101** 030401
[29] Fischbach E and Talmadge C L 1999 *T*he Search for Non-Newtonian Gravity (New York: AIP/Springer-Verlag)
[30] Gundlach J H 2005 *New J. Phys.* **7** 205
[31] Onofrio R 2006 *New J. Phys.* **8** 237

[32] Serry F M, Walliser D, and Maclay G J 1995 *J. Microelectromech. Syst.* **4** 193
[33] Buks E and Roukes M L 2001 *Europhys. Lett.* **24** 220; 2001 *Phys. Rev. B* **63** 033402
[34] Chan H B, Aksyuk V A, Kleiman R N, Bishop D J, and Capasso F 2001 *Phys. Rev. Lett.* **87** 211801
[35] Kim W J, Brown-Hayes M, Dalvit D A R, Brownell J H, and Onofrio R 2008 *Phys. Rev. A* **78** 020101(R)
[36] Stipe B C, Mamin H J, Stowe T D, Kenny T W, and Rugar D 2001 *Phys. Rev. Lett.* **87** 096801
[37] Speake C C and Trenkel C 2003 *Phys. Rev. Lett.* **90** 160403
[38] Brown-Hayes M, Dalvit D A R, Mazzitelli F D, Kim W J, and Onofrio R 2005 *Phys. Rev. A* **72** 052102
[39] Dalvit D A R, Lombardo F C, Mazzitelli F D, and Onofrio R 2004 *Europhys. Lett.* **67** 517
[40] Albrecht T R, Gr̈utter P, Horne D, and Rugar D 1991 *J. Appl. Phys.* **69** 668; Kim B I 2004 *Rev. Sci. Instr.* **75** 5035
[41] Timoshenko S, Young D H and Weaver W Jr. 1974 *V*ibration Problems in Engineering (New York: Wyley)
[42] Rugar D, Marmin H J, and Guethner P 1989 *Appl. Phys. Lett.* **55** 2588
[43] Lamoreaux S K 2008 E-Print arXiv:0808.0885v1 [quant-ph] 6 Aug 2008
[44] García R and Pérez R 2002 *Surface Sci. Rep.* **47** 197
[45] Iannuzzi D, Lisanti M, and Capasso F 2004 *Proc. Nat. Ac. Sci. USA* **101** 4019.
[46] Sader J E *et al.* 1995 *Rev. Sci. Instrum.* **66** 3789
[47] Cappella B and Dietler G 1999 *Surf. Sci. Rep.* **34** 1
[48] Bressi G, Carugno G, Galvani A, Onofrio R, Ruoso G, and Veronese F 2001 *Class. Quantum Grav.* **18** 3943
[49] Albrecht T R *et al.* 1991 J. Appl. Phys. **69** 668
[50] Giessibl F 2003 *Rev. Mod. Phys.* **75** 949
[51] Boyer L *et al.* 1994 J. Phys. D **27** 1504
[52] Decca RS, Fischbach E, Klimchitskaya GL, Krause DE, Lopez D, Mohideen U, and Mostepanenko VM 2008 e-print arXiv:0809.3576v1 [quant-ph]
[53] Lifshitz E M 1956 *Sov. Phys. - JETP* **2** 73; Lifshitz E M and Pitaevskii L P 1980 *S*tatistical Physics, Part 2 (Oxford: Pergamon Press)
[54] Palik E D (editor) 1995 *H*andbook of Optical Constants of Solids (New York: Academic Press)
[55] Chiu H-C, Chang C-C, Castillo-Garza R, Chen F, and Mohideen U 2008 *J. Phys. A* **41** 164022
[56] Pollack S E, Schlamminger S, and Gundlach J H 2008 *Phys. Rev. Lett.* **101** 071101
[57] Onofrio R and Carugno G 1995 *Phys. Lett. A* **198** 365
[58] Chen F, Klimchitskaya, Mohideen U., and Mostepanenko V M 2004 *Phys. Rev. A* **69** 022117
[59] Binnig G, Quate C F, and Gerber Ch 1986 *Phys. Rev. Lett.* **56** 930
[60] Weaver J M R and Abraham D W 1991 *J. Vac. Sci. Techn. B* **9** 1559
[61] Terris B D, Stern J E, Rugar D, and Mamin H J 1989 *Phys. Rev. Lett.* **63** 2669
[62] Blackman G S, Mate C M, and Philpott M R 1990 *Phys. Rev. Lett.* **65** 2270
[63] Burnham N A, Colton R J, and Pollock H M 1992 *Phys. Rev. Lett.* **69** 144
[64] Dürig U, Züger O, and Pohl D W 1990 *Phys. Rev. Lett.* **65** 349
[65] Dürig U and Züger O 1994 *Phys. Rev. B* **50** 5008
[66] Hargreaves C M 1969 *Phys. Lett. A* **30** 491
[67] Volokitin A I and Persson B N 2003 *Phys. Rev. B* **68** 155420
[68] Dorofeyev I, Fuchs F, Gotsmann B, and Wenning G 1999 *Phys. Rev. B* **60** 9069
[69] Gotsmann B, Seidel C, Anczykowski B, and Fuchs H 1999 *Phys. Rev. B* **60** 11051
[70] Loppacher C *et al.* 2000 *Phys. Rev. B* **62** 13674
[71] Pfeiffer O, Nony L, Bennewitz R, Baratoff A, and Meyer E 2004 *Nanotechnology* **15** 101
[72] Volokitin A I, Persson B N J and Ueba H 2006 *Phys. Rev. B* **73** 165423
[73] Israelachvili J N and Tabor D 1972 *Proc. R. Soc. London, Series A, Math. and Phys. Sci.* **331** 4435
[74] Robertson M A *et al.* 2006 *Class. Quant. Grav.* **23** 2665
[75] Palacios-Lidon E and Colchero J 2006 *Nanotechnology* **17** 5491
[76] Munday J and Capasso F 2007 *Phys. Rev. A* **75** 060102(R)
[77] de Man S, Heeck K, and Iannuzzi D 2008 e-print arXiv:0809.3858v1 [quant-ph]; J. Chevrier (*private communication*); S.K. Lamoreaux (*private communication*); G. Palasantzas (*private communication*)